Article:

The Journal of Physiology

Na$^+$ current properties in islet α- and β-cells reflect cell-specific *Scn3a* and *Scn9a* expression

Quan Zhang[1], Margarita V. Chibalina[1], Martin Bengtsson[1], Lukas N. Groschner[1], Reshma Ramracheya[1], Nils J. G. Rorsman[1], Veronika Leiss[2,3], Mohammed A. Nassar[4,5], Andrea Welling[2], Fiona M. Gribble[6], Frank Reimann[6], Franz Hofmann[2,7], John N. Wood[4], Frances M. Ashcroft[8] and Patrik Rorsman[1,9]

[1] *Oxford Centre for Diabetes, Endocrinology and Metabolism, University of Oxford, Churchill Hospital, Oxford OX3 7LJ, UK*

[2] *Institut für Pharmakologie und Toxikologie, TU München, Biedersteiner Str. 29, 80802, München, Germany*

[3] *Institut für Pharmakologie und Toxikologie, Eberhard-Karls Universität, Wilhelmstr. 56, 72074, Tübingen, Germany*

[4] *Molecular Nociception Group, University College London (UCL), Gower Street, London WC1E 6BT, UK*

[5] *Biomedical Science, University of Sheffield, Sheffield S10 2TN, UK*

[6] *Cambridge Institute for Medical Research, University of Cambridge School of Clinical Medicine, Wellcome Trust/MRC Building, Cambridge Biomedical Campus, Hills Road, Cambridge CB2 0XY, UK*

[7] *FOR 923, Institut für Pharmakologie und Toxikologie, TU München, Biedersteiner Str. 29, 80802, München, Germany*

[8] *Henry Wellcome Centre for Gene Function, Department of Physiology, Anatomy and Genetics, University of Oxford, Parks Road, Oxford OX1 3PT, UK*

[9] *Department of Neuroscience and Physiology, Sahlgren's Academy, University of Göteborg, Box 430, SE40530, Göteborg, Sweden*

Key points

- α- and β-cells express both Na$_v$1.3 and Na$_v$1.7 Na$^+$ channels but in different relative amounts.
- The differential expression explains the different properties of Na$^+$ currents in α- and β-cells.
- Na$_v$1.3 is the functionally important Na$^+$ channel α subunit in both α- and β-cells.
- Islet Na$_v$1.7 channels are locked in an inactive state due to an islet cell-specific factor.

Mouse pancreatic β- and α-cells are equipped with voltage-gated Na$^+$ currents that inactivate over widely different membrane potentials (half-maximal inactivation ($V_{0.5}$) at -100 mV and -50 mV in β- and α-cells, respectively). Single-cell PCR analyses show that both α- and β-cells have Na$_v$1.3 (*Scn3*) and Na$_v$1.7 (*Scn9a*) α subunits, but their relative proportions differ: β-cells principally express Na$_v$1.7 and α-cells Na$_v$1.3. In α-cells, genetically ablating *Scn3a* reduces the Na$^+$ current by 80%. In β-cells, knockout of *Scn9a* lowers the Na$^+$ current by >85%, unveiling a small *Scn3a*-dependent component. Glucagon and insulin secretion are inhibited in *Scn3a$^{-/-}$* islets but unaffected in *Scn9a*-deficient islets. Thus, Na$_v$1.3 is the functionally important Na$^+$ channel α subunit in both α- and β-cells because Na$_v$1.7 is largely inactive at physiological membrane potentials due to its unusually negative voltage dependence of inactivation. Interestingly, the Na$_v$1.7 sequence in brain and islets is identical and yet the $V_{0.5}$ for inactivation is >30 mV more negative in β-cells. This may indicate the presence of an intracellular factor that modulates the voltage dependence of inactivation.

Introduction

Insulin and glucagon are the principal hormones involved in glucose homeostasis. They are secreted from the β- and α-cells, respectively, of the pancreatic islets in response to changes in plasma glucose levels, with insulin secretion being stimulated and glucagon secretion being suppressed by glucose elevation (Ashcroft & Rorsman, 2013). The regulation of their release is impaired in diabetes mellitus: insulin secretion is insufficient and glucagon levels are inappropriately elevated (Dunning *et al.* 2005; Ashcroft & Rorsman, 2012). In both cell types, electrical activity is crucial for hormone release (Ashcroft & Rorsman, 2013). This electrical activity is orchestrated by the concerted activity of several different types of ion channel (Rorsman *et al.* 2011).

Voltage-gated Na$^+$ channels play a central role in cellular excitability (Hille, 2001). They are dually influenced by the membrane potential. A large rapid depolarization results in Na$^+$ channel opening and an inward Na$^+$ current. However, if depolarization is sustained, the channel enters a non-conducting 'inactivated' state, resulting in a decline in current flow. Thus, the magnitude of the Na$^+$ current depends on the potential at which the membrane normally sits.

Mammalian Na$^+$ channels consist of a pore-forming α subunit and auxiliary β subunits that modify channel gating (Catterall, 2000). There are nine different genes (*Scn1a-5a* and *Scn8a-11a*) that encode Na$^+$ channel α subunits (Catterall *et al.* 2005). The channels resulting from these genes are named Na$_v$1.1–Na$_v$1.9 (Goldin *et al.* 2000). Confusingly, the numbers of the genes and the protein do not always match. Thus, Na$_v$1.6 and Na$_v$1.7 are encoded by the genes *Scn8a* and *Scn9a*, respectively (Goldin *et al.* 2000). Currently, four isoforms of the β subunits are known: referred to as *Scn1b*, *Scn2b*, *Scn3b* and *Scn4b* (Koopmann *et al.* 2006). With few exceptions (Na$_v$1.5, Na$_v$1.8 and Na$_v$1.9; Catterall *et al.* 2005), voltage-gated Na$^+$ channels are sensitive to the neurotoxin TTX.

Pancreatic islet cells are equipped with TTX-sensitive voltage-gated Na$^+$ channels (Gopel *et al.* 2000*a*,*b*; Vignali *et al.* 2006). Na$^+$ channels are critical for glucose-induced electrical activity and insulin secretion in human β-cells (Pressel & Misler, 1990; Braun *et al.* 2008). However, their role in rodent β-cells is puzzling because they exhibit an arcane voltage dependence of inactivation. Surprisingly, when holding at membrane potentials found under physiological conditions, depolarisation evokes almost no Na$^+$ current in β-cells (Plant, 1988; Gopel *et al.* 1999; Lou *et al.* 2003). By contrast, large Na$^+$ currents can be evoked in α-cells held at physiological membrane potentials and blocking these channels with TTX slows the upstroke of the action potential and inhibits glucagon secretion (Zhang *et al.* 2013).

It has been proposed that the different inactivation properties of Na$^+$ currents in α- and β-cells are attributable to different α or β subunit composition (Lou *et al.* 2003). Here, we tested this hypothesis using a combination of biophysical measurements of islet cell Na$^+$ currents and single-cell PCR analyses. The functional significance of the different Na$^+$ channel α subunits on electrical activity and hormone secretion was dissected using mice in which specific α subunits were genetically deleted.

Our data confirm the important role of Na$^+$ channels in glucagon secretion, and provide evidence for a previously unrecognised role for Na$^+$ channels in insulin secretion. They also raise the possibility that β-cells contain a factor that shifts the voltage dependence of inactivation of Na$_v$1.7 Na$^+$ channels to hyperpolarised levels, rendering the channel functionally inactive at physiological membrane potentials.

Methods

Ethics

All animal experiments were conducted in accordance with the UK Animals Scientific Procedures Act (1986) and University of Oxford ethical guidelines. Human pancreatic islets were isolated with ethical approval and clinical consent at the Diabetes Research and Wellness Foundation Human islet Isolation Facility (Oxford).

Animals

Unless otherwise indicated, all experiments were performed using islets from C57BL/6 mice (wild-type). Global Na$_v$1.3 (*Scn3a$^{-/-}$*) knockout mice were generated as described previously (Nassar *et al.* 2006). These mice were healthy, fertile and grew as well as their littermate wild type controls (Nassar *et al.* 2006). To generate α- and β-cell-specific Na$_v$1.7-deficient mice, *Scn9a$^{+/L2}$* mice carrying one modified (L2) allele and one wild-type allele (Nassar *et al.* 2004) were crossed with mice expressing *Cre*-recombinase under the control of the rat glucagon promoter (*GlucCre$^{+/tg}$*; Herrera, 2000) or the rat insulin 2 promoter (*RipCre$^{+/tg}$*; Postic *et al.* 1999). The resulting *Scn9a$^{+/L2}$GlucCre$^{+/tg}$* or *Scn9a$^{+/L2}$RipCre$^{+/tg}$* mice were mated with *Scn9a$^{L2/L2}$* mice homozygous for the modified L2 allele. This gave rise to α-cell-specific (*Scn9a$^{L2/L2}$GlucCre$^{+/tg}$*) and β-cell-specific (*Scn9a$^{L2/L2}$RipCre$^{+/tg}$*) knockout mice (here referred to as α-*Scn9a$^{-/-}$* and β-*Scn9a$^{-/-}$* mice, respectively) as well as to littermate control animals *Scn9a$^{+/L2}$GlucCre$^{+/tg}$* or *Scn9a$^{+/L2}$RipCre$^{+/tg}$* (referred to as α-*Scn9a$^{+/-}$* or as β-*Scn9a$^{+/-}$*). The background mouse strain was C57BL/6. The *in vivo* phenotype of the α- and β-cell-specific

Scn9a$^{-/-}$ mice was not characterised but they were not overtly diabetic, consistent with the mild effects on secretion observed *in vitro*.

One series of experiments (see Fig. 5*A*) was performed on tdRFP-negative cells in islets from mice expressing the red fluorescent protein (tdRFP) under the control of the somatostatin promoter (see supplementary material in Chera *et al.* 2014). It was ascertained that tdRFP-expressing cells contain somatostatin.

Preparation of pancreatic islets

Mice were killed by cervical dislocation, the pancreases quickly removed and islets isolated by collagenase digestion. Islets were used for acute experiments and were not maintained in tissue culture for more than 16 h.

Whole-cell patch-clamp recordings

Whole-cell Na$^+$ currents were recorded in α- and β-cells within intact islets using the standard whole-cell configuration as previously described (Gopel *et al.* 1999). The measurements were performed using EPC-9 or EPC-10 patch-clamp amplifiers and Pulse software (HEKA Electronics, Lambrecht/Pfalz, Germany). Currents were compensated for capacitive transients and linear leak using a $-P/4$ protocol. The currents were filtered at 2.9 kHz and digitised at >10 kHz.

The standard extracellular medium for the electrophysiological measurements consisted of (mM) 118 NaCl, 20 tetraethylammonium-Cl (TEA-Cl), 5.6 KCl, 1.2 MgCl$_2$, 5 Hepes (pH 7.4 with NaOH), 2.6 CaCl$_2$, 5 D-glucose and 2 CoCl$_2$ (to block Ca^{2+} channels). The pipette solution contained (mM) 120 CsCl, 1 MgCl$_2$.6H$_2$O, 1 CaCl$_2$, 10 EGTA, 10 Hepes (pH 7.15 with CsOH) and 3 Mg-ATP. TTX (Alomone Labs, Jerusalem, Israel) was used at a final concentration of 0.1 μg ml^{-1}.

Membrane potential recordings were performed as described previously (De Marinis *et al.* 2010) using the perforated-patch technique and K$_2$SO$_4$-filled electrodes. In these experiments, the extracellular (Krebs–Ringer buffer, KRB) solution consisted of (mM) 140 NaCl, 3.6 KCl, 0.5 MgSO$_4$, 0.5 NaH$_2$PO$_4$, 2 NaHCO$_3$, 5 Hepes, 1.5 CaCl$_2$ and glucose as indicated. All electrophysiological experiments were performed at 34°C.

Hormone measurements

Batches of 10–20 size-matched islets were preincubated in 0.3 ml of a modified KRB containing 1 mM glucose and 2 mg ml^{-1} BSA for 1 h at 37°C, followed by a 1 h test incubation in 0.3 ml of the same medium supplemented with glucose, receptor antagonists, metabolic inhibitors and ion channel activators/blockers as indicated. Insulin and glucagon were assayed using Millipore RI-3K (Billerica, MA, USA) and Eurodiagnostica RB 306 (Malmö, Sweden) radioimmunoassays, respectively. The somatostatin receptor (SSTR) antagonist BIM23056 was obtained from Tocris (Bristol, UK).

Pancreas perfusion

Dynamic measurements of insulin secretion were performed using *in situ* pancreatic perfusion. Briefly, the aorta was cannulated by ligating above the coeliac artery and below the superior mesenteric artery, and the pancreas was perfused with KRB solution at a rate of $\sim$0.45 ml min^{-1} using an Ismatec (Glattbrugg, Switzerland) Reglo Digital MS2/12 peristaltic pump. The perfusate was maintained at 37°C with a Warner Instruments temperature control unit TC-32 4B in conjunction with a tube heater (Warner Instruments P/N 64-0102, Hamden, CT, USA) and a Harvard Apparatus (Holliston, MA, USA) heated rodent operating table. The effluent was collected, using a Teledyne (Thousand Oaks, CA, USA) ISCO Foxy R1 fraction collector, by cannulating the portal vein. The pancreas was first perfused for 20 min with 1 mM glucose before commencing the experiment to establish the basal rate of secretion.

[Ca^{2+}]$_i$ imaging

Confocal [Ca^{2+}]$_i$ imaging experiments were conducted essentially as previously reported (Girard *et al.* 2009). Islets were superfused with the KRB described above plus glucose and TTX or tolbutamide as indicated, at a flow rate of 1 ml min^{-1} and 37°C.

Identification of α- and β-cells in intact islets

In all voltage-clamp experiments, the identity of the α-cells was established by immunocytochemistry following injection of the cell with biocytin (0.5 mg ml^{-1}) via the recording electrode (Zhang *et al.* 2007). In the membrane potential recordings, α-cells were identified based on their spontaneous action potential firing with 1 mM glucose; β-cells were identified as cells that were electrically silent and hyperpolarized with 1 mM glucose and had characteristic oscillatory electrical activity when exposed to 8 mM glucose (Gopel *et al.* 2000*a*). Cells identified by these criteria had Na$^+$ channel inactivation properties characteristic of α- and β-cells, as indicated by voltage-clamp measurements in cells identified by immunocytochemistry. For [Ca^{2+}]$_i$ measurements, β-cells were identified by the induction of [Ca^{2+}]$_i$ oscillations at 6 mM glucose that convert into a (more) sustained [Ca^{2+}]$_i$ elevation at 20 mM glucose.

RNA purification and quantitative RT-PCR

RNA purification and quantitative RT-PCR in mouse islet cells were carried out as described elsewhere (Braun *et al.* 2009, 2010). Details of primer sequences used will be provided on request. Some experiments were performed using mRNA collected from α- and β-cell fractions purified by fluorescence-activated cell sorting, as described previously (De Marinis *et al.* 2010)

Preamplification and single-cell RT-PCR

Individual cells were collected using 2 μl 0.5% NP-40 lysis buffer. cDNA was synthesized as above with a reaction volume of 10 μl (Bengtsson *et al.* 2005; Stahlberg & Bengtsson, 2010). Single-cell cDNA was preamplified for 10 cycles with the TaqMan PreAmp Master Mix Kit (PN4364130, Applied Biosystems, Foster City, CA, USA) and TaqMan assays according to the manufacturer's instructions. In the subsequent quantitative PCR (qPCR), 2.5 μl preamplification product diluted 1:20 was used. The presence of transcript was defined as a positive signal from the TaqMan probe after 40 PCR cycles. Amplicon size was confirmed by agarose gel electrophoresis.

Identification of *Scn9a* splice variants in mouse islets

Total RNA purified from mouse islets and brain was reverse-transcribed using a High Capacity RNA-to-cDNA Kit (Applied Biosystems). PCR was performed with *Scn9a* gene-specific primers and the resulting PCR products were cloned using a Zero Blunt TOPO PCR cloning kit (Invitrogen, Carlsbad, CA, USA) and sequenced.

Data analysis

All data are given as mean values $\pm$ SEM of the indicated number of experiments (n).

All electrophysiological experiments were performed on the indicated number of cells obtained (unless otherwise stated) from at least three different animals (usually more). Current amplitudes have been normalised to cell capacitance and are expressed as pA pF^{-1}. Inactivation was analysed by applying 200 ms conditioning pulses (from -180 to -5 mV) followed by a test pulse to 0 mV (applied at a frequency of 1 Hz). Peak current amplitude during the test pulse (I) was normalized to that observed when the conditioning pulse went to -180 mV (I_{max}). Data are presented as h_∞ ($= I/I_{max}$). The Na$^+$ current activation parameters were determined as described previously (Gonoi & Hille, 1987): the Na$^+$ conductance (G) was calculated from the measured Na$^+$ current amplitudes (I) by the relation $G = I/(V - V_r)$ where V is the membrane potential and V_r is the estimated reversal potential (Nernst

potential), calculated from the extra- and intracellular Na$^+$ concentrations in media used. Values of G at a given V were normalised to the maximal G (G_{max}). Inactivation and activation curves were fit to single or double Boltzmann functions as appropriate. Peak current amplitudes, the activation (τ_m) and inactivation (τ_h) time constants, and inactivation properties were estimated using the electrophysiology analysis software package Pulsefit (Heka Electronics. Lamprecht/Pfalz, Germany).

Action potential peak voltages were measured as reported elsewhere (Zhang *et al.* 2013); the number of action potentials for each experimental condition/cell averaged >40.

Statistical significances were evaluated using Student's *t* test or ANOVA (for multiple comparisons), as appropriate.

Results

Molecular characterization of Na$^+$ channel subunits in mouse and human pancreatic islets

In mouse pancreatic islets, *Scn9a* was the dominant α subunit, being expressed at levels 6-fold higher than *Scn3a* and *Scn8a*. Of the β subunits, only *Scn1b* and *Scn3b* were detected (Fig. 1*A*). The high expression of *Scn9a* and *Scn1b* in islets is in agreement with a previous report (Ernst *et al.* 2009).

We performed single-cell PCR to determine which subunits are expressed in α- and β-cells, respectively (Fig. 1*B*). All cells used for this analysis possessed voltage-gated Na$^+$ currents, as confirmed by whole-cell patch-clamp recordings prior to mRNA collection. Yet most cells (40 out of a total of 52 β-cells and 24 out of a total of 37 α-cells, from three mice) lacked detectable mRNA for any of the Na$^+$ channel α subunits, perhaps due to low mRNA copy numbers and/or non-continuous gene transcription (Raj *et al.* 2006). In those α-cells in which transcripts were detected, *Scn3a* and *Scn9a* were found equally often. Importantly, 2 of the 13 α-cells contained mRNA for both *Scn3a* and *Scn9a*. In β-cells (Fig. 1*B*, lower), *Scn9a* was the most abundant transcript (4.5-fold more frequent than *Scn3a*). No β-cells and only one α-cell expressed *Scn8a*. Of the β subunits, *Scn3b* was found 2.7-fold more often than *Scn1b* in α-cells, whereas *Scn1b* predominated in β-cells (detected 4.5-fold more often than *Scn3b*).

We also measured Na$^+$ channel transcripts in pure α- and β-cell fractions. In α-cells (Fig. 1*C*, top), *Scn9a* was the most abundant transcript but relatively high levels of *Scn3a* and *Scn8a* were also found. Among the β subunits, *Scn3b* was predominantly expressed (>4-fold higher than *Scn1b*). In β-cells (Fig. 1*C*, bottom), *Scn9a* was expressed at levels 7- to 20-fold higher than *Scn8a* and *Scn3a*, respectively, and *Scn1b* was expressed at 6-fold higher levels than *Scn3b*. In agreement with the whole-islet data, β subunits were expressed at much lower levels than

Scn9a in both α- and β-cell fractions. Thus, the data obtained from purified α- and β-cell populations are in good agreement with those obtained from single α- and β-cells.
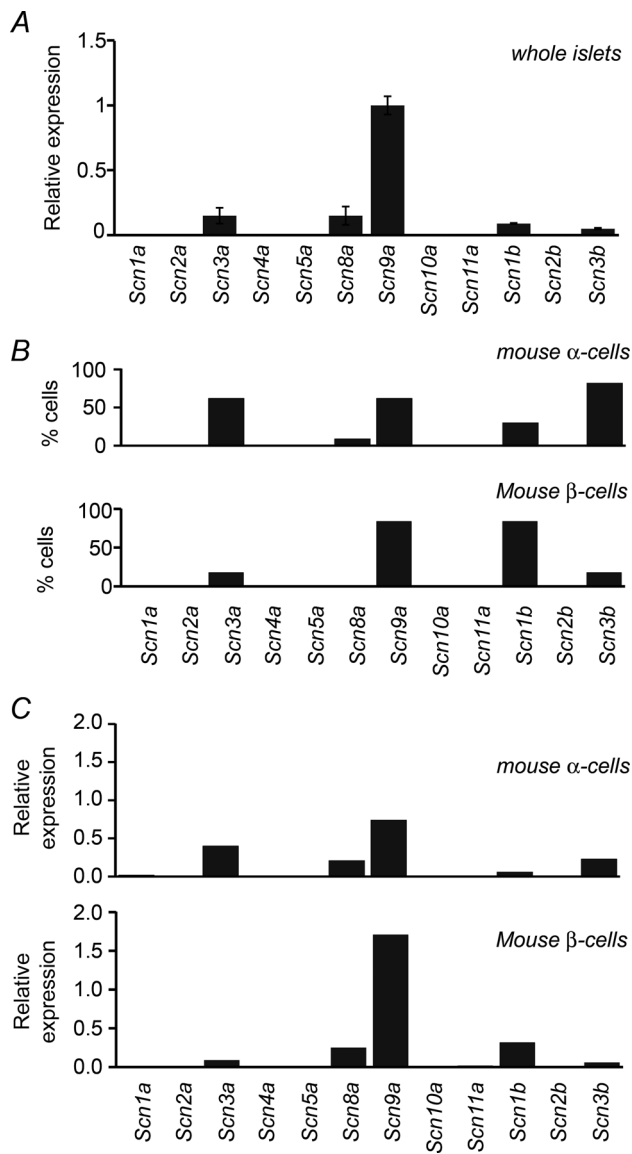

Figure 1. Expression of Na$^+$ channel subunits in pancreatic islet cells

A, qPCR on mouse islets ($n = 3$ preparations). Data have been normalized to expression of *Scn9a*, which in turn was normalised against mean expression of ribosomal protein S29 (*Rps29*) and hypoxanthine guanine phosphoribosyl transferase 1 (*Hprt*). *B*, single-cell PCR analyses of α- (top) and β-cells (lower). Data are presented as the percentage of α-cells (or β-cells) containing the indicated Na$^+$ channel transcript and come from 13 α-cells (identified by the presence of glucagon mRNA), and 12 β-cells (containing insulin mRNA). Cells come from three mice. *C*, as in *A* but using pure α- (top) and β-cell fractions (lower).

Properties of Na$^+$ currents in mouse α- and β-cells

As our PCR analyses indicated that α- and β-cells may contain Na$^+$ channels of different molecular composition, we next investigated whether this might give rise to biophysically distinct Na$^+$ currents. All electrophysiological data reported here were obtained from identified α or β-cells in intact acutely isolated pancreatic islets. In β-cells, two types of responses were observed. In 70% of β-cells (7/10 cells), no Na$^+$ current was seen when the holding potential was -70 mV but large Na$^+$ currents were evoked when the cells were subsequently hyperpolarised to -180 mV. In the remaining β-cells ($n = 3$), voltage-gated Na$^+$ currents were elicited from -70 mV that increased only $\sim$2-fold when the cells were hyperpolarised to -180 mV. Figure 2*A* compares the mean Na$^+$ *I–V* relationship evoked from holding potentials of -70 or -180 mV.

We analysed the voltage dependence of Na$^+$ current inactivation using a standard two-pulse protocol (Fig. 2*B*). In most β-cells ($n = 7$), inactivation was well described by a single Boltzmann function with half-maximal inactivation ($V_{0.5}$) at -97 ± 1 mV. However, in the subset of cells in which Na$^+$ currents could be evoked from -70 mV, inactivation was best described as a sum of two Boltzmann functions with $V_{0.5}$ at -97 ± 6 and -50 ± 1 mV, comprising 49 ± 10 and $51 \pm 10\%$ of the maximum current, respectively ($n = 3$). When the data from all 10 cells were pooled, inactivation was biphasic with $V_{0.5}$ at -95 ± 2 and -50 ± 1 mV, comprising 85 ± 8 and $15 \pm 8\%$ of the maximum current, respectively (Fig. 2*B*).

In α-cells, large Na$^+$ currents were invariably observed when holding at -70 mV and hyperpolarization to -180 mV only marginally increased ($+20\%$) the peak current amplitude (Fig. 2*C*). Figure 2*C* compares the *I–V* relationships recorded when cells were held at -70 or -180 mV. A biphasic inactivation curve was observed in all 6 cells analysed (Fig. 2*D*). The more negative component had a $V_{0.5}$ of -84 ± 5 mV and accounted for only $26 \pm 3\%$ of the total Na$^+$ current. The principal component (comprising $74 \pm 3\%$) had a $V_{0.5}$ of -47 ± 1 mV.

Also shown in Fig. 2*B* and *D* are the Na$^+$ current activation curves. In α-cells, activation was monotonic and half-maximal at -23 ± 2 mV ($n = 6$). In the subset of β-cells where part of the Na$^+$ current inactivated at more positive membrane potentials, activation was also monotonic and half-maximal at -23 ± 1 mV ($n = 3$). The corresponding value in β-cells where all Na$^+$ current inactivated at more negative voltages ($V_{0.5} \sim -100$ mV) was -24 ± 3 mV ($n = 7$). The activation curve shown in Fig. 2*B* is based on the data from all 10 β-cells.

The finding that all α-cells (and some β-cells) exhibit biphasic voltage-dependent Na$^+$ current inactivation suggests that Na$^+$ channel subunits with widely different inactivation properties are coexpressed in individual

cells. This echoes the single-cell PCR measurements that provided direct evidence for the expression of both *Scn3a* and *Scn9a* within the same α-cell.

Families of voltage-clamp currents recorded from β- and α-cells during membrane depolarisation from −180 to −20, −10 and 0 mV are shown in Fig. 3*A* and *B*. The voltage dependence of the time constants of activation (τ_m) and inactivation (τ_h) of the Na$^+$ currents in α- and β-cells are compared in Fig. 3*C* and *D*. In both α- and β-cells, inactivation became progressively more rapid (seen as a decrease in τ_h) as the cells were depolarised. The differences between α- and β-cells were subtle but τ_h was higher in β-cells at voltages above −10 mV.

Role of Na$^+$ channels in islet cell electrical activity: effects of TTX

The inactivation properties of the β-cell Na$^+$ currents suggest that Na$^+$ channels will be almost fully inactivated at physiological membrane potentials in β-cells and thus contribute little (if at all) to β-cell electrical activity and hormone secretion. By contrast, Na$^+$ channels are likely to be functionally more important in glucagon-secreting α-cells. We examined this idea by performing membrane potential recordings from α- and β-cells within intact pancreatic islets, using the perforated patch configuration (in which cell metabolism remains intact).

Unlike β-cells, α-cells are electrically active at 1 mM glucose (Zhang *et al.* 2013). Figure 4*A* shows α-cell action potentials displayed on a slow (left) and expanded (right) time base under control conditions, during application of the Na$^+$ channel blocker TTX (0.1 μg ml^{-1}) and following washout of the toxin. TTX consistently reduced the peak voltage of the action potentials: from $+2 \pm 5$ mV ($n = 6$) to -12 ± 1 mV ($P < 0.01$). Thus, Na$^+$ channels are important for the upstroke of the action potential in α-cells.

In β-cells, TTX had more variable effects. In 3 out of 6 cells, TTX barely affected action potential firing elicited by 8 mM glucose (Fig. 4*B*). However, in the remaining three
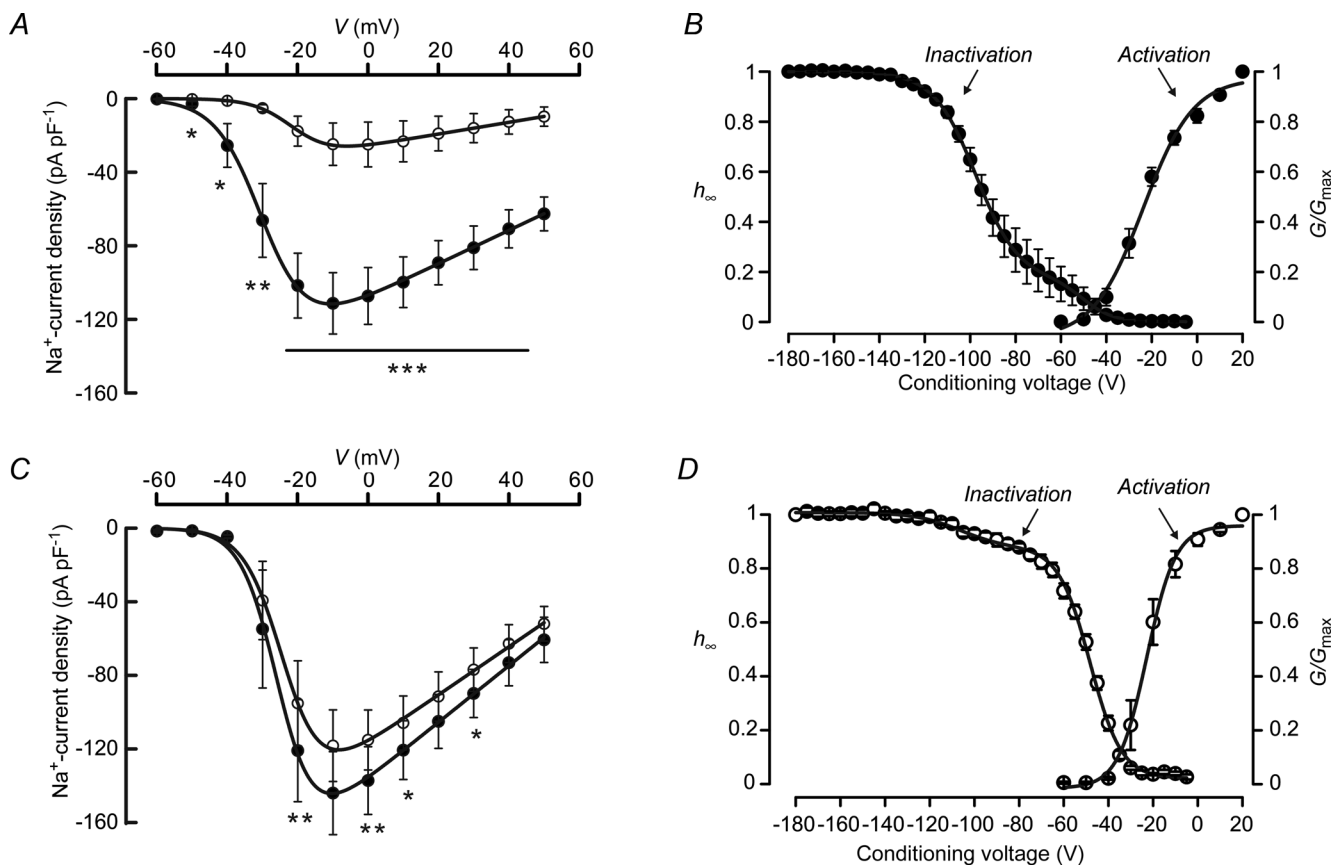

Figure 2. Properties of voltage-gated Na$^+$ currents in α- and β-cells in intact islets
A, *I*–*V* relationships recorded from holding potentials of −70 mV (○) or −180 mV (●) in β-cells ($n = 10$). Cells were depolarised to voltages between −60 and +50 mV in 10 mV increments. Note that the more hyperpolarized holding potential leads to the generation of large Na$^+$ currents. *B*, voltage dependence of Na$^+$ current inactivation (h_∞) and activation (G/G_{max}) in β-cells. The curves represent a double Boltzmann fit to the data ($n = 10$). *C* and *D*, as in *A* and *B* but experiments were conducted on α-cells ($n = 6$). *P < 0.05, **P < 0.01, ***P < 0.001 for differences between holding at −70 and −180 mV.

β-cells, TTX markedly reduced action potential amplitude (Fig. 4C): peak voltage decreased from -8 ± 1 mV in the absence to -20 ± 3 mV in the presence of TTX ($n = 3$; $P < 0.03$, paired t test). When all six cells were averaged, peak voltage decreased from -18 ± 5 to -24 ± 2 mV, but this difference did not quite reach statistical significance ($P < 0.07$, paired t test).

In the presence of 20 mM glucose (Fig. 4D), when β-cells were permanently depolarised to a membrane potential of -47 ± 1 mV, TTX reduced the peak action potential voltage from -25 ± 7 to -29 ± 6 mV ($n = 4$; $P < 0.05$, paired t test). Note that whereas slow membrane potential oscillations sometimes persist in β-cells exposed to 20 mM glucose (as exemplified by the cell shown in Fig. 4D), the response to the higher glucose concentration more often consists of nearly uninterrupted action potential firing without lengthy repolarised electrically silent intervals (not shown but see Kanno *et al.* 2002)

Effects of TTX on glucose-induced [Ca^{2+}]$_i$ increases in β-cells and insulin secretion

In β-cells, action potential firing culminates in the opening of voltage-gated Ca^{2+} channels. We tested the effects of glucose and TTX on β-cell [Ca^{2+}]$_i$ by confocal imaging in fluo4-loaded mouse islets (Fig. 5A). In most cells (104 out of 110 cells) in which [Ca^{2+}]$_i$ was low and stable at 1 mM glucose, increasing glucose to 6 mM did not induce any [Ca^{2+}]$_i$ oscillations whereas a subsequent increase to 20 mM elicited a sustained elevation of [Ca^{2+}]$_i$ (Fig. 5A, i).

However, in a small subset of cells ($n = 6$), [Ca^{2+}]$_i$ oscillations were evoked by 6 mM glucose. In these cells, addition of TTX reversibly reduced the frequency of the [Ca^{2+}]$_i$ oscillations from 2.0 ± 0.7 to 0.5 ± 0.2 min^{-1} ($P < 0.05$) and decreased the area under the curve (above baseline) by $72 \pm 14\%$ ($P < 0.05$). Increasing glucose further, from 6 to 20 mM, resulted in a more sustained elevation of [Ca^{2+}]$_i$ (Fig. 5A, ii). The frequency of the rapid [Ca^{2+}]$_i$ oscillations observed at threshold glucose concentrations, and their conversion to a non-oscillatory sustained increase at higher glucose levels, echos the effects of glucose on β-cell electrical activity (Henquin & Meissner, 1984). In intact islets, β-cells are electrically coupled by gap junctions and this synchronises electrical activity and [Ca^{2+}]$_i$ oscillations in a K$_{ATP}$ channel-dependent fashion (Rocheleau *et al.* 2006). Unlike what is seen at higher glucose concentrations (Zhang *et al.* 2008), the [Ca^{2+}]$_i$ oscillations observed
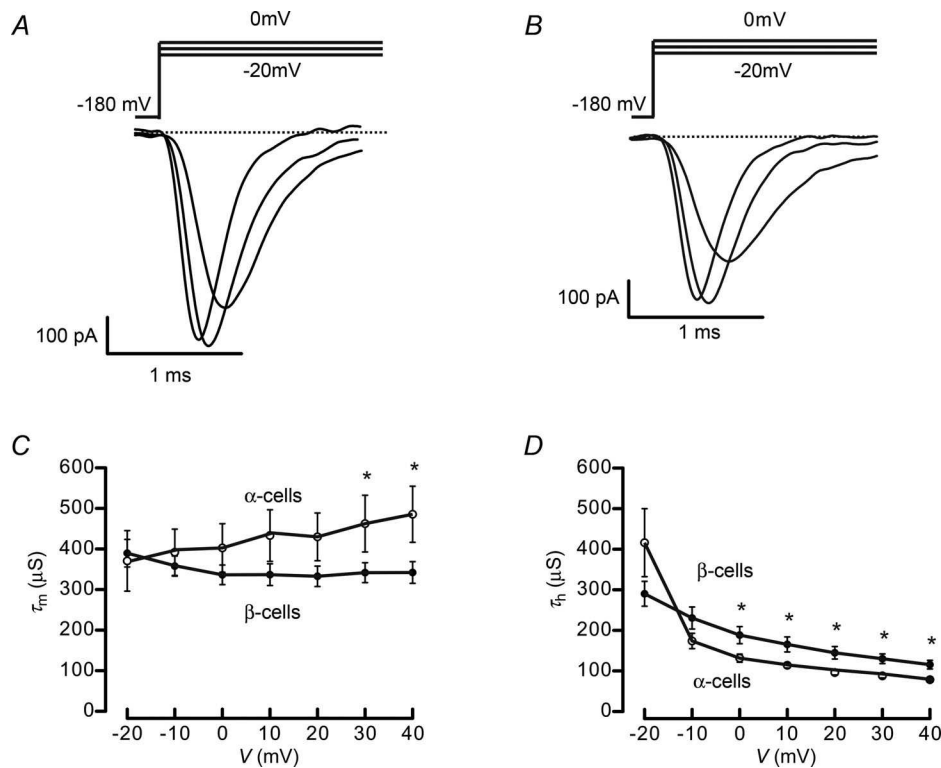

Figure 3. Voltage dependence of Na$^+$ current amplitude and kinetics in islet cells
A, family of voltage-clamp currents evoked by depolarisations from -180 to -20, -10 and 0 mV in a β-cell. *B*, as in *A* but currents were recorded from an α-cell. *C*, time constant of activation (τ_m) recorded from β-cells ($\bullet$; $n = 5$) and α-cells ($\circ$; $n = 5$) during depolarisations to membrane potentials between -20 and $+40$ mV. *D*, as in *C* but for the time constant of inactivation (τ_h). *$P < 0.05$.

at 6 mM glucose were not well synchronised across the islet (Fig. 5*B*). It is possible that this is a consequence of the K_{ATP} channel activity being slightly greater in the non-active cells and that the lower input resistance prevents synchronisation of electrical activity mediated by current spread via the gap junctions.

We acknowledge that we cannot exclude the possibility that some of the cells responding to 6 mM glucose were somatostatin-secreting δ-cells, which have a lower threshold for secretion than β-cells. To test this possibility, we performed experiments on islets from mice expressing red fluorescent protein (tdRFP) under the control of the somatostatin promoter. Some tdRFP-negative cells (likely to be β-cells) responded to 6 mM glucose with TTX-sensitive $[Ca^{2+}]_i$ oscillations that converted to

a sustained elevation when glucose was subsequently increased to 20 mM (Fig. 5*A*, *iii*). The oscillatory pattern in tdRFP-positive cells (i.e. δ-cells) was rather different and consisted of larger and more regular $[Ca^{2+}]_i$ oscillations that were easily distinguished from those seen in β-cells. Interestingly, ~30% of tdRFP-positive δ-cells exhibited spontaneous $[Ca^{2+}]_i$ oscillations at 1 mM glucose (Fig. 5*A*, *iv*). Collectively, the data suggest that a small number of β-cells are indeed active at 6 mM glucose.

We next examined the effects of TTX on insulin secretion using the perfused mouse pancreas preparation (Fig. 5*C*, *D*). Under control conditions, increasing glucose from 1 to 6 mM evoked a transient ~7-fold stimulation of insulin secretion (Fig. 5*C*, *D*). It is likely that this is released from the small subset of β-cells that show
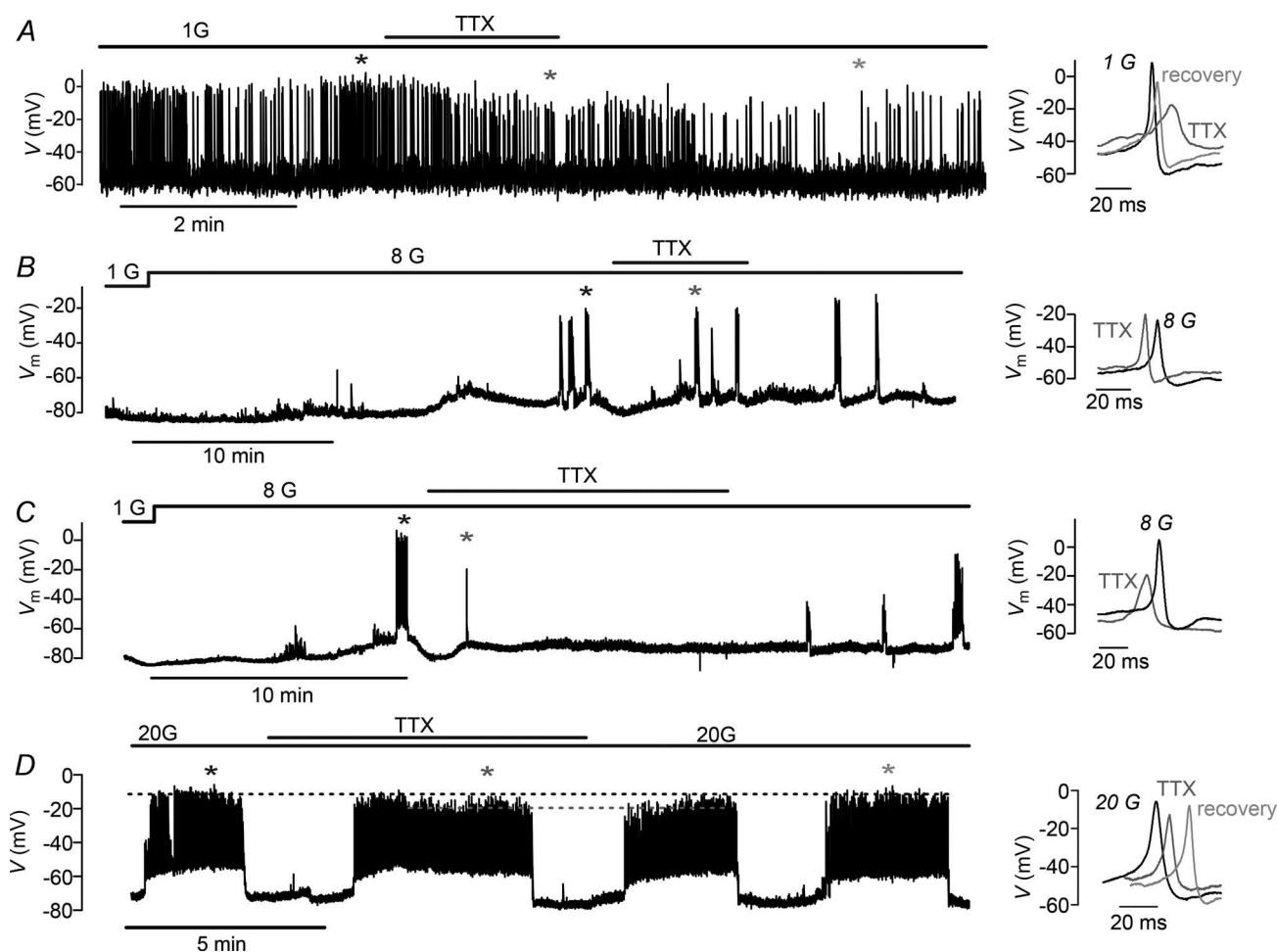

Figure 4. Effects of TTX on α- and β-cell electrical activity
A, *left*, membrane potential recording from an α-cell in an intact mouse pancreatic islet exposed to 1 mM glucose before and after addition of TTX (0.1 μg ml⁻¹), as indicated. *Right*, examples of action potentials recorded before, during and after TTX application shown on an expanded time base. *B* and *C*, *left*, membrane potential recordings from β-cells in intact islets exposed to 1 or 8 mM glucose and TTX, as indicated. Examples of responses in which TTX had little effect (*B*; *n* = 3) or where it suppressed glucose-induced electrical activity (*C*; *n* = 3). *Right*, examples of action potentials (recorded at the time points indicated by the black and grey stars) recorded at 8 mM glucose in the absence and presence of TTX. *D*, *left*, effects of TTX on β-cell electrical activity evoked by 20 mM glucose. *Right*, examples of action potentials recorded at 20 mM glucose in the absence and presence of TTX (*n* = 4).
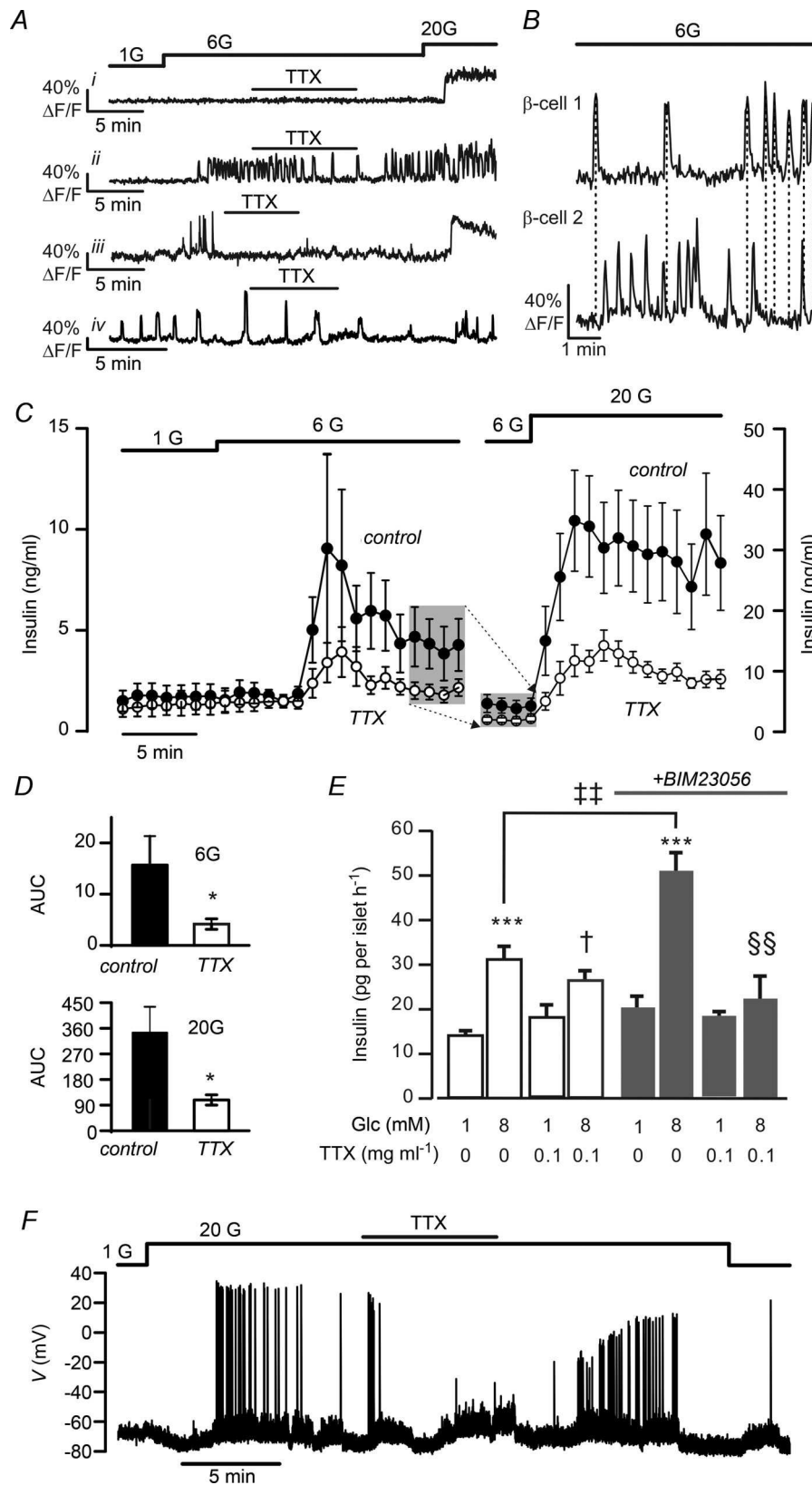
Figure 5. Effects of TTX on [Ca²⁺]ᵢ and insulin secretion

A, [Ca²⁺]ᵢ responses recorded from single cells in intact islets. Glucose (1, 6 or 20G) and TTX were applied as indicated above the top trace (same for all recordings). *i*, example of a cell that did not respond to 6 mM glucose

$[Ca^{2+}]$ oscillations in 6 mM glucose (Fig. 5A, ii and iii). Subsequent stimulation with 20 mM glucose evoked an insulin secretory response that was >20-fold higher than that elicited by 6 mM glucose (Fig. 5C, D). This correlated with an 18-fold increase in the number of cells showing $[Ca^{2+}]_i$ oscillations. Thus, it seems that much of the increase in glucose-dependent insulin secretion reflects recruitment of additional β-cells. At both 6 and 20 mM glucose, insulin secretion was strongly inhibited by the Na^+ channel blocker TTX: the inhibitory effect averaged 74 ± 8 and $68 \pm 7\%$, respectively (Fig. 5D).

The strong suppression of glucose-induced insulin secretion by TTX seen in the perfused pancreas experiments (Fig. 5D) contrasts with the weaker effect of TTX on glucose-induced insulin secretion found in static incubations of isolated islets (Fig. 5E, left). Somatostatin-secreting δ-cells possess large TTX-sensitive voltage-gated Na^+ currents (Gopel *et al.* 2000a). As expected, δ-cells identified by expression of tdRFP generated large (100 mV) over-shooting action potentials when exposed to 20 mM glucose, and these were reversibly suppressed by TTX (Fig. 5F). We reasoned that TTX-induced suppression of somatostatin secretion might result in relief from paracrine inhibition of insulin secretion in static incubations (Renstrom *et al.* 1996; Hauge-Evans *et al.* 2009). To test this hypothesis, we compared insulin secretion in the absence and presence of the SSTR subtype 5 (SSTR5) antagonist BIM23056 (SSTR5 is the predominant SSTR subtype in mouse β-cells; Strowski *et al.* 2003). The SSTR5 antagonist stimulated insulin secretion at 8 mM glucose by ≥50% (Fig. 5E, right). While TTX had little effect in the absence of BIM23056, it exerted a strong inhibitory effect (≥60%) in its presence. By contrast, in the perfused mouse pancreas, BIM23056

did not increase glucose-induced insulin secretion (data not shown).

Collectively, the data of Figs 4 and 5 suggest that Na^+ channels play a previously unrecognised role in the initiation of β-cell electrical activity, $[Ca^{2+}]_i$ oscillations and insulin secretion. We next attempted to establish the molecular identity of these Na^+ channels.

Na⁺ currents in *Scn3a⁺ᐟ⁻* and *Scn3a⁻ᐟ⁻* α- and β-cells

Expression analysis (Fig. 1) suggests that $Na_v1.3$ (*Scn3a*) might contribute to the Na^+ current in both β- and α-cells. We examined this possibility by comparing α- and β-cell Na^+ currents in cells from heterozygous *Scn3a⁺ᐟ⁻* (that contain one functional *Scn3a* allele) and *Scn3a⁻ᐟ⁻* knockout mice (that contain no functional alleles).

Figure 6A shows Na^+ current I–V relationships for *Scn3a⁺ᐟ⁻* and *Scn3a⁻ᐟ⁻* β-cells. The magnitude of the Na^+ current in *Scn3a⁺ᐟ⁻* β-cells was slightly smaller than in wild-type β-cells (compare with Fig. 2A) but this difference was not statistically significant. However, that in *Scn3a⁻ᐟ⁻* β-cells was reduced by ~35%. Figure 6B compares the voltage dependence of Na^+ current inactivation in β-cells from *Scn3a⁺ᐟ⁻* and *Scn3a⁻ᐟ⁻* mice. Biphasic inactivation was observed in 4 of the 7 *Scn3a⁺ᐟ⁻* β-cells analysed: one component, accounting for $69 \pm 20\%$ of the current, inactivated with a $V_{0.5}$ of -94 ± 5 mV and a second component, comprising $31 \pm 20\%$, inactivated with a $V_{0.5}$ of -49 ± 7 mV. In the remaining 3 cells, inactivation was monophasic with a $V_{0.5}$ of -94 ± 3 mV. Mean data from all seven *Scn3a⁺ᐟ⁻* β-cells are shown in Fig. 6B. These values are not significantly different from those of wild-type β-cells (Fig. 2B). In *Scn3a⁻ᐟ⁻* β-cells,

but where 20 mM glucose elicited a sustained increase in $[Ca^{2+}]_i$. This trace is representative of 104 of 110 cells in 9 islets from 4 different mice. *ii*, example of a cell that responded with TTX-sensitive $[Ca^{2+}]_i$ oscillations when exposed to 6 mM glucose (6 of 110 cells). Subsequent elevation of glucose to 20 mM resulted in a more sustained increase in $[Ca^{2+}]_i$. *iii*, recording from a β-cell (identified by the *absence* of tdRFP fluorescence) in an islet from an Sst-tdRFP mouse that generated $[Ca^{2+}]_i$ oscillations at 6 mM glucose and a sustained $[Ca^{2+}]_i$ elevation when glucose was increased to 20 mM. *iv*, recording from a δ-cell (identified by the *presence* of tdRFP fluorescence); note the large, regular spontaneous $[Ca^{2+}]_i$ oscillations at 1 mM glucose which are little affected by increasing the glucose concentration (unlike what is seen in β-cells). *B*, poor synchronization of $[Ca^{2+}]_i$ oscillations in β-cells exposed to 6 mM glucose. The traces were taken from two β-cells in the same islet. The dotted vertical lines indicate the peaks of the $[Ca^{2+}]_i$ oscillations in cell 1. *C*, stimulation of insulin secretion by 6 mM (left) and 20 mM (right) glucose in the absence (●; $n = 8$) or presence (○; $n = 9$) of TTX (0.1 μg ml⁻¹). Note the different ordinate scales. The grey areas highlight the same data points displayed using the different ordinate scales. For clarity, statistical significances are not shown. *D*, area under the curve (AUC) measured in response to 6 or 20 mM glucose in the absence and presence of TTX (0.1 μg ml⁻¹; as indicated). Note the different ordinate scales for 6 and 20 mM glucose. *$P < 0.05$ ($n = 8$–9). *E*, insulin secretion measured at 1 or 8 mM glucose (Glc) with or without TTX in the absence (left) or presence (right) of 100 nM BIM23056 ($n = 6$–8 replicates using islets from eight mice). ***$P < 0.001$ *vs.* 1 mM glucose alone; †$P < 0.01$ *vs.* 1 mM glucose and TTX; ‡‡$P < 0.01$ *vs.* 8 mM glucose; §§$P < 0.01$ *vs.* 8 mM glucose and BIM23056. *F*, reversible suppression of action potential firing by TTX in a tdRFP-expressing δ-cell. Note stimulation of action potentials when glucose was increased from 1 to 20 mM (1G and 20G). TTX was applied at a concentration of 0.1 μg ml⁻¹ as indicated by the bold horizontal line.

inactivation was invariably monophasic and occurred with a $V_{0.5}$ of -102 ± 2 mV ($n = 18$).

The amplitude of the Na$^+$ current in *Scn3a$^{+/-}$* α-cells was slightly smaller than that observed in control animals (compare Figs 2A and 6C) but this difference was not statistically significant. Figure 6C shows I–V relationships recorded from *Scn3a$^{+/-}$* and *Scn3a$^{-/-}$* α-cells using a holding potential of -180 mV. Total ablation of *Scn3a* reduced the maximum current by ~85% compared to that observed in *Scn3a$^{+/-}$* α-cells.

As in wild-type α-cells (Fig. 2D), Na$^+$ current inactivation was biphasic in all *Scn3a$^{+/-}$* α-cells ($n = 11$, Fig. 6D). One component, comprising $24 \pm 10\%$ of the total current, inactivated at negative voltages ($V_{0.5} = -91 \pm 2$ mV) and another component, accounting for $76 \pm 10\%$ of the total current, inactivated at more positive voltages ($V_{0.5} = -38 \pm 2$ mV). These values are comparable to those observed in wild-type cells (Fig. 2D). In *Scn3a$^{-/-}$* α-cells, the Na$^+$ current component inactivating at voltages above -50 mV was abolished and the relationship was well described by a single Boltzmann function with a $V_{0.5}$ of -94 ± 7 mV ($n = 5$). However, there was a hint of a small component of inactivation between

-90 and -50 mV that may represent *Scn8a*, expression of which was detected in α-cells (see Fig. 1).

Influence of ablating *Scn3a* on Na$^+$ current kinetics

We examined the consequence of *Scn3a* ablation on the time constants of activation (τ_m) and inactivation (τ_h) in α- and β-cells. Activation and inactivation kinetics in *Scn3a$^{+/-}$* α-cells were similar to those observed in wild-type α-cells (compare Figs 7A and B and 3C and D). Ablation of *Scn3a* slowed activation (increased τ_m; Fig. 7A) and accelerated inactivation (reduced τ_h; Fig. 7B). In β-cells, ablation of *Scn3a* did not measurably affect Na$^+$ current kinetics, presumably because *Scn3a*/Na$_v$1.3 only accounts for a fraction (<20%) of the β-cell Na$^+$ current.

Na$^+$ currents in *β-Scn9a$^{-/-}$* β-cells

We next measured Na$^+$ currents after cell-specific knockout of *Scn9a* (Na$_v$1.7). Figure 8A shows I–V relationships recorded from *β-Scn9a$^{+/-}$* and *β-Scn9a$^{-/-}$*
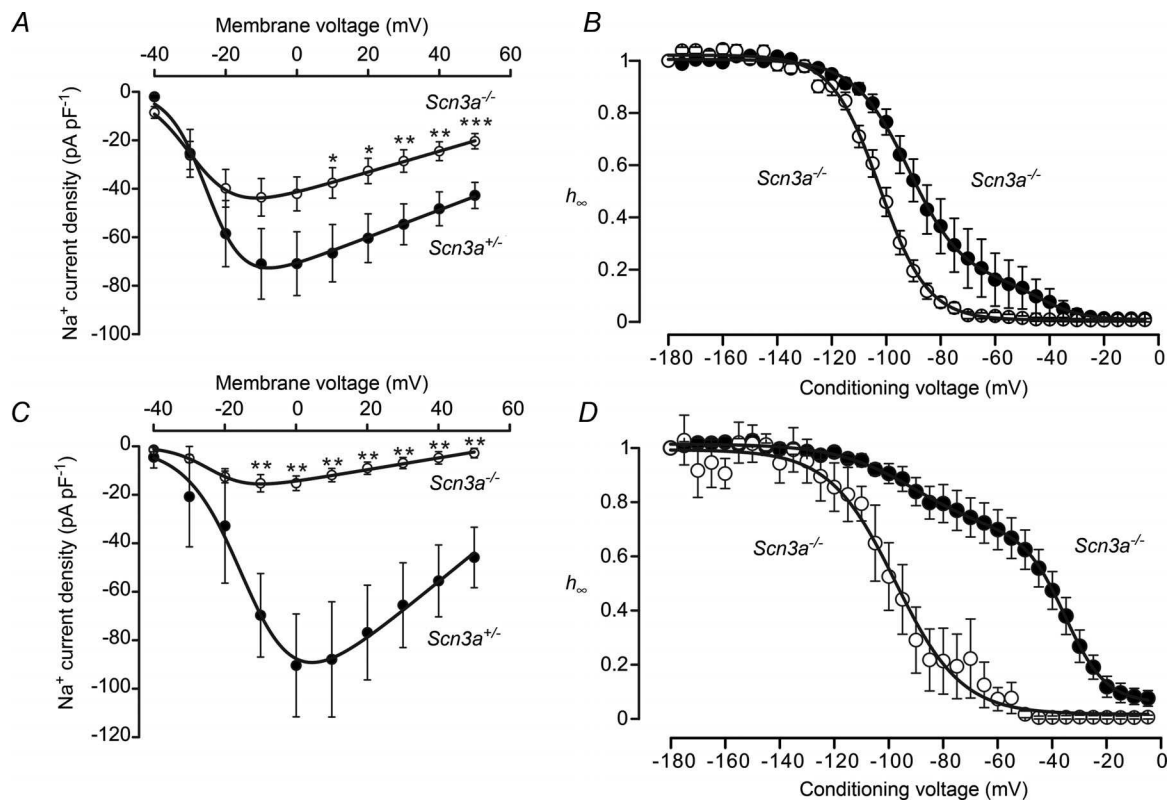
Figure 6. Effects of ablating *Scn3a* on Na$^+$ currents in α- and β-cells
A, peak Na$^+$ I–V relationships for *Scn3a$^{+/-}$* (●; $n = 6$) and *Scn3a$^{-/-}$* (○; $n = 12$) β-cells. *$P < 0.05$, **$p < 0.01$, ***$p < 0.001$ vs. responses in *Scn3a$^{+/-}$* β-cells. B, voltage-dependence of Na$^+$ current inactivation in *Scn3a$^{+/-}$* (●; $n = 7$) and *Scn3a$^{-/-}$* β-cells (○; $n = 18$). C and D, as in A and B but experiments were performed on α-cells (C: $n = 4$ for *Scn3a$^{+/-}$* and $n = 6$ for *Scn3a$^{-/-}$*; D: $n = 11$ for *Scn3a$^{+/-}$* and $n = 7$ for *Scn3a$^{-/-}$*). The curves are the best fit of single (*Scn3a$^{-/-}$*) and double (*Scn3a$^{+/-}$*) Boltzmann functions to the data points. *$P < 0.05$ vs. *Scn3a$^{+/-}$*.

β-cells. All β-cells from β-Scn9a$^{+/-}$ mice contained large Na$^+$ currents ($n = 8$) with an amplitude comparable to that observed in wild-type mice (compare Figs 2A and 8A). By contrast, Na$^+$ currents were seen in only 5 of the 14 β-Scn9a$^{-/-}$ β-cells and the average maximum peak current in all 14 cells (including those lacking detectable Na$^+$ currents) was accordingly reduced by 85%.

Figure 8B compares the voltage dependence of Na$^+$ current inactivation in β-Scn9a$^{+/-}$ and β-Scn9a$^{-/-}$ β-cells. In most β-Scn9a$^{+/-}$ β-cells, there was a single component of inactivation with a $V_{0.5}$ of -100 ± 2 mV. However, a small additional component (with a $V_{0.5}$ of -49 ± 7 mV) was seen in 4 of the 14 cells studied. This amounted to <10% of the total current and gave rise to a very small (5–10% of the total current) shoulder on the inactivation curve at voltages positive to -80 mV. In β-Scn9a$^{-/-}$ β-cells, the Na$^+$ current inactivation could be described by a single Boltzmann function and was half-maximal at -66 ± 7 mV ($n = 4$).

Na$^+$ currents in α-Scn9a$^{-/-}$ α-cells

We next measured Na$^+$ currents after α-cell-specific knockout of *Scn9a*. Figure 8C illustrates the I–V

relationships for *Scn9a*$^{+/-}$ and *Scn9a*$^{-/-}$ α-cells. Ablation of *Scn9a* reduced the Na$^+$ current amplitude by <10%; the residual current inactivated with a $V_{0.5}$ of ~ -35 mV (data not shown), in reasonable agreement with that obtained for the principal Na$^+$ current component observed in wild-type α-cells (Fig. 2D). Na$^+$ current activation and inactivation kinetics in α-Scn9a$^{+/-}$ and α-Scn9a$^{-/-}$ α-cells were identical (data not shown), presumably because Na$^+$ current kinetics in α-cells are principally determined by non-Na$_v$1.7 channels (probably Na$_v$1.3). We conclude that Na$_v$1.7 Na$^+$ channels contribute only marginally to the α-cell Na$^+$ current.

Influence of ablating Scn9a on Na$^+$ current kinetics

Na$^+$ current activation and inactivation kinetics in β-Scn9a$^{+/-}$ and β-Scn9a$^{-/-}$ β-cells are compared in Fig. 9. In β-Scn9a$^{+/-}$ β-cells, Na$^+$ current kinetics were comparable to those seen in wild-type β-cells (Fig. 3C and D). Whereas the effects on inactivation (τ_h) were not statistically significant, activation tended to be slower in β-Scn9a$^{-/-}$ β-cells and τ_m measured at -10 mV increased from ~ 0.3 to ~ 0.7 ms. No effects on Na$^+$ current kinetics were seen in α-Scn9a$^{-/-}$ α-cells (data not shown),
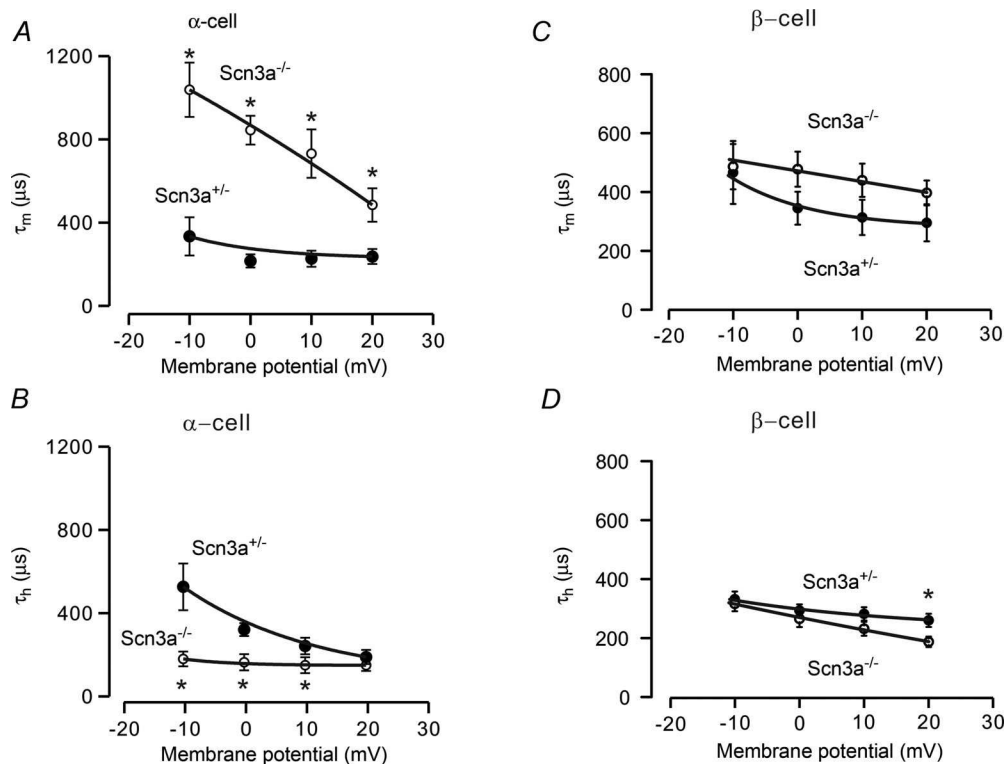
Figure 7. Activation and inactivation of Na$^+$ currents in *Scn3a*$^{+/-}$ and *Scn3a*$^{-/-}$ α- and β-cells
A, time constant of activation (τ_m) recorded from *Scn3a*$^{+/-}$ (●; $n = 5$) and *Scn3a*$^{-/-}$ α-cells (○; $n = 5$) during depolarisations to membrane potentials between -10 and $+20$ mV. B, as in A but measuring the time constant of inactivation (τ_h). *$P < 0.05$ for difference between *Scn3a*$^{+/-}$ and *Scn3a*$^{-/-}$ α-cells. C and D, as in A and B but experiments were made in β-cells ($n = 5$).

presumably reflecting the small contribution of $Na_v1.7$ Na^+ channels to the α-cell Na^+ current.

Effects of *Scn3a* and *Scn9a* ablation on glucagon and insulin secretion

Our electrophysiological analyses reveal that *Scn3a* encodes a Na^+ channel ($Na_v1.3$) that is active at physiological membrane potentials and thus suggest that ablation

A, peak Na^+ *I–V* relationships for β-*Scn9a*$^{+/-}$ (●; $n = 8$) and β-*Scn9a*$^{-/-}$ β-cells (○; $n = 15$ from one mouse). *$p < 0.05$, **$p < 0.01$, ***$P < 0.001$ *vs.* β-*Scn9a*$^{+/-}$ data. **B**, voltage dependence of Na^+ current inactivation in β-*Scn9a*$^{-/-}$ (○; $n = 9$; from one mouse) and β-*Scn9a*$^{+/-}$ (●; $n = 15$) β-cells. The curves are the best fits of a single (β-*Scn9a*$^{-/}$) or double (β-*Scn9a*$^{+/-}$) Boltzmann function to the data. **C**, as in **A** but for α-cells in α-*Scn9a*$^{+/-}$ (·; $n = 8$) and α-*Scn9a*$^{-/-}$ islets (○; $n = 8$). *$P < 0.05$ *vs.* α-*Scn9a*$^{+/-}$.

of $Na_v1.3$ channels will influence electrical activity and hormone secretion in both α- and (some) β-cells. Conversely, ablation of *Scn9a*, which encodes a Na^+ current that inactivates at negative membrane potentials, is predicted to have little (if any) effect on glucagon or insulin secretion.

In *Scn3a*$^{+/-}$ islets, increasing glucose from 1 to 8 mM inhibited glucagon secretion by >60% (Fig. 10*A*, left), similar to what is observed in wild-type islets (not shown here but see Macdonald *et al.* 2007). In *Scn3a*$^{-/-}$ islets (Fig. 10*A*, right), glucagon secretion at 1 mM glucose was reduced by two-thirds compared to that seen in *Scn3a*$^{+/-}$ islets and although elevating glucose to 8 mM resulted in further suppression, the magnitude of this effect was reduced by 70%. The lower rate of glucagon secretion in *Scn3a*-deficient islets was not due to a decreased glucagon content, which averaged 939 ± 99 and 804 ± 23 pg per islet in *Scn3a*$^{+/-}$ and *Scn3a*$^{-/-}$ islets, respectively (not statistically different).

Whereas TTX inhibited glucagon secretion at 1 mM glucose in *Scn3a*$^{+/-}$ islets, it was without inhibitory effect in *Scn3a*$^{-/-}$ islets: if anything, it tended to stimulate glucagon secretion (Fig. 10*A*), possibly reflecting relief from paracrine inhibition (cf. Zhang *et al.* 2013).

Ablation of *Scn9a* in α-cells did not affect glucagon secretion at either 1 or 10 mM glucose (Fig. 10*B*) and TTX was equally inhibitory at 1 mM glucose in both control *Scn9*$^{+/-}$ and *Scn9a*$^{-/-}$ islets (Fig. 10*B*).

In both *Scn3a*$^{+/-}$ and β-*Scn9a*$^{+/-}$ islets, glucose (8 or 10 mM) stimulated insulin secretion ~3-fold (Fig. 10*C* and *D*, left). However, glucose failed to stimulate insulin secretion in *Scn3a*-deficient islets (Fig. 10*C*, right) although it remained stimulatory in β-*Scn9a*$^{-/-}$ islets (Fig. 10*D*).
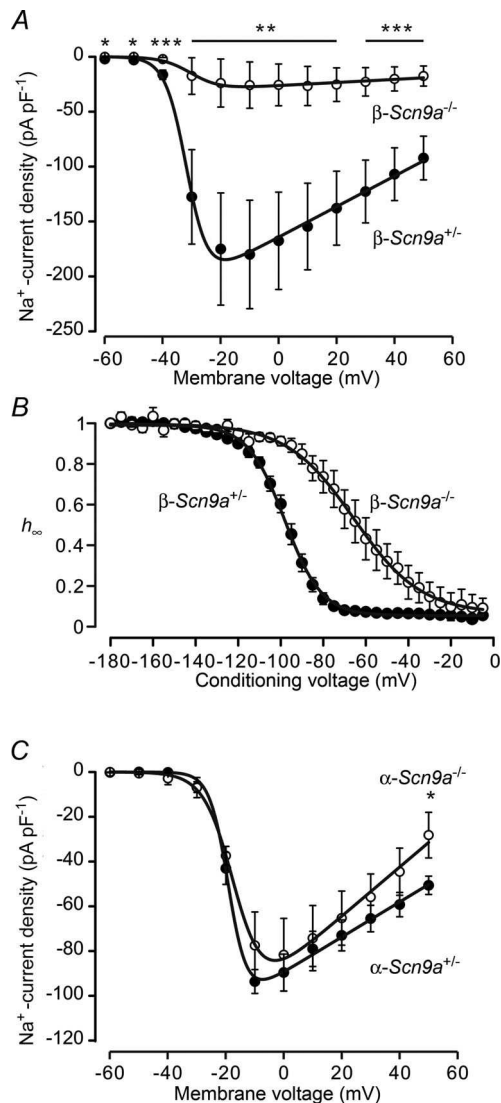
Pancreatic islets do not express an islet-specific *Scn9a* isoform

The inactivation of $Na_v1.7$ Na^+ channels (encoded by *Scn9a*) we observe in mouse β-cells occurs at voltages 30 mV more negative than reported for the same channels in sensory neurones (Herzog *et al.* 2003). One possible explanation for this discrepancy is that β-cells and neurones express distinct $Na_v1.7$ isoforms. However, although two splice variants were detected in both mouse islets and brain tissue, named isoforms A and B (Fig. 11), their deduced amino acid sequences were 100% identical.

$Na_v1.7$ inactivation is controlled by an intracellular islet cell factor

$Na_v1.7$ heterologously expressed in HEK 293 cells inactivates with a $V_{0.5}$ of -70 mV (Cox *et al.* 2006), which

Figure 8. Effects of ablating *Scn9a* on Na^+ currents in α- and β-cells

is 30–40 mV more positive than we observe in β-cells. The finding that $Na_v1.7$ is identical in islets and brain therefore suggests that islet cells contain a factor that shifts $Na_v1.7$ inactivation toward unphysiologically negative membrane potentials. We tested the possible involvement of a diffusible (cytosolic) factor by comparing Na^+ current inactivation in β-cells at various times after establishment of the whole-cell configuration. We measured $V_{0.5}$ as -98 ± 1 and -104 ± 1 mV ($n = 3$; $P < 0.02$) at 2 and 15 min after starting the recordings, respectively (Fig. 12A). It is evident that the shift is small and in the opposite direction, and thus cannot explain why Na^+ channel inactivation occurs at such negative voltages in β-cells.

Na$^+$ channel inactivation in human β-cells

Unlike rodent β-cells, Na^+ currents in human β-cells are reported to inactivate at physiological membrane potentials (Misler *et al.* 1992; Braun *et al.* 2008). Recent RNA sequencing data indicate that *SCN9A* represents a small fraction (25%) of Na^+ channel transcripts on human β-cells (Nica *et al.* 2013). We therefore reassessed the voltage dependence of inactivation in human β-cells. Two components of inactivation were observed in 4 out of 9 human β-cells: one component accounting for $23 \pm 3\%$ of the current inactivated with a $V_{0.5}$ of -105 ± 2 mV and a second component comprising $77 \pm 3\%$ with a $V_{0.5}$ of -41 ± 1 mV. In the remaining 5 cells, inactivation was monotonic with a $V_{0.5}$ of -46 ± 1 mV (Fig. 12B). The contribution of the component inactivating at negative voltage averaged $10 \pm 4\%$ of the total Na^+ current when data from all nine cells were combined. Its smallness probably explains why it escaped detection in the earlier study (Braun *et al.* 2008).

Discussion

Our data demonstrate that α- and β-cells express the same types of voltage-dependent sodium channel α subunits: $Na_v1.3$ (*Scn3a*) and $Na_v1.7$ (*Scn9a*). Although *Scn8a* ($Na_v1.6$) is also expressed in both α- and β-cells, electrophysiological data indicate that $Na_v1.6$ channels do not contribute substantially to the Na^+ current in either cell type.

Na^+ channel density in the plasma membrane (measured as the maximum Na^+ current that can be evoked from a hyperpolarized membrane potential) is approximately equal for both cell types but Na^+ currents evoked from physiological resting potentials are far larger in α-cells (100 pA pF^{-1}) than β-cells (20 pA pF^{-1}). The reason for this difference is that the relative expression of $Na_v1.3$ and $Na_v1.7$ differs, with $Na_v1.3$ being expressed at high levels in α-cells and $Na_v1.7$ being the dominant subtype in β-cells. Furthermore, $Na_v1.7$ channels in both α- and β-cells are locked in a functionally inactive state, so that they contribute little to the physiologically activatable Na^+ current density. Thus, in β-cells, where $Na_v1.7$ dominates, little Na^+ current can be evoked from physiological resting potentials. As a consequence, $Na_v1.7$ plays a relatively minor functional role in β-cells, despite the fact that it accounts for 80–90% of the transcripts. In α-cells, by contrast, where $Na_v1.3$ dominates, large Na^+ currents can be activated at physiological membrane potentials (-60 mV) and blocking Na^+ channels with TTX abolishes the stimulation of glucagon secretion evoked by low glucose (Zhang *et al.* 2013).

Mouse α- and β-cells express different Na$^+$ channel subunits: impact on Na$^+$ channel inactivation

Although *Scn9a*/$Na_v1.7$ is expressed in both α- and β-cells (Vignali *et al.* 2006), we observed that *Scn9a* is quantitatively far more important in β-cells than α-cells
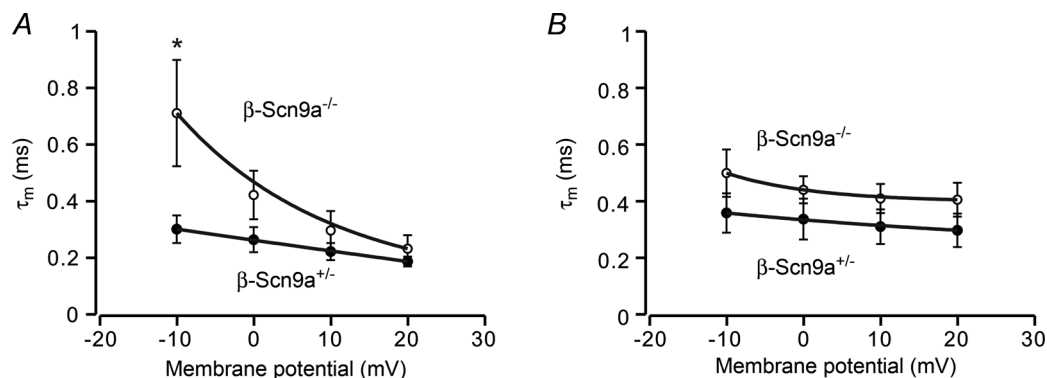
Figure 9. Activation and inactivation of Na$^+$ currents in β-Scn9a$^{+/-}$ and β-Scn9a$^{-/-}$ β-cells
A, time constant of activation (τ_m) recorded from β-Scn9a$^{+/-}$ (•; $n = 8$) and β Scn9a$^{-/-}$ β-cells (○; $n = 4$) during depolarisations to membrane potentials between -10 and $+20$ mV. B, as in A but measuring the time constant of inactivation (τ_h). *$P < 0.05$.

(>80 vs. 45% of all Na$^+$ channel transcripts, respectively). In agreement with this finding, 80–90% of the β-cell Na$^+$ current flows through Na$_v$1.7 channels, but only 10–20% of the α-cell Na$^+$ current. Conversely, Na$_v$1.3 is more important in α-cells, in terms of both transcripts (30–50%) and Na$^+$ current density (70–90%). Thus, there is a reasonable agreement between the electrophysiological and molecular biological data.

Role of Na$^+$ channels in β-cells

We found that the Na$^+$ channel blocker TTX inhibited electrical activity, [Ca^{2+}]$_i$ and insulin secretion in the perfused pancreas. These data are in apparent disagreement with our previous finding that insulin secretion is little affected by TTX in isolated mouse islets (Macdonald et al. 2007). We attribute this discrepancy to accumulation of secreted somatostatin during static incubations of isolated islets, which leads to suppression of insulin secretion. By blocking somatostatin secretion, we hypothesise that TTX relieves the paracrine inhibition of insulin secretion and that this effect masks the suppression of insulin secretion produced by inhibition of Na$^+$ channels in β-cells. Indeed, when somatostatin signalling in β-cells was pharmacologically prevented, insulin secretion in isolated islets became TTX-sensitive (Fig. 5E).

At first sight, a major role for voltage-gated Na$^+$ channels in β-cell electrical activity and insulin secretion seems unlikely given that the Na$^+$ current is almost fully (>90%) inactivated at −70 mV, which is close to the most negative membrane potential attained in the absence of glucose. However, 30% of β-cells possess a component of Na$^+$ current that inactivates only at more positive potentials. Inactivation of this current is half-maximal at ~−50 mV, which is comparable to the plateau potential from which the action potential originates at glucose concentrations ≥20 mM. Although
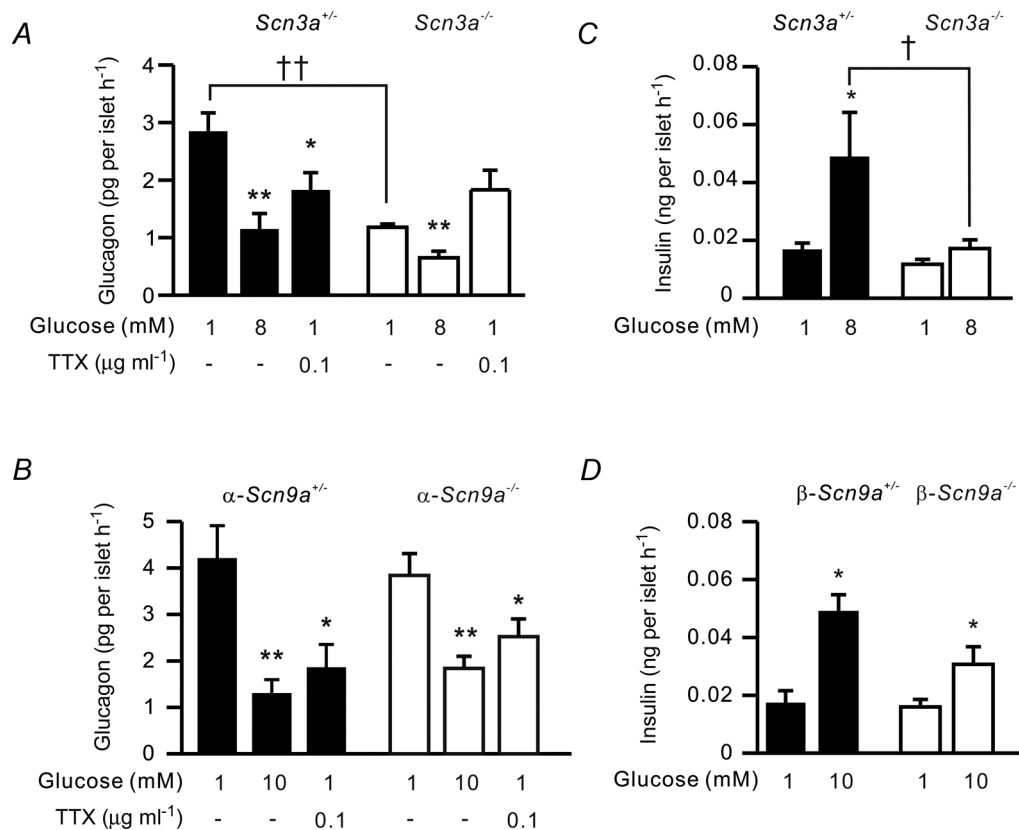

Figure 10. **Effects of ablating *Scn3a* and *Scn9a* on insulin and glucagon secretion**
A, glucagon secretion measured during 1 h static incubations at the indicated concentrations of glucose and TTX from *Scn3a*$^{+/−}$ (left) and *Scn3a*$^{−/−}$ (right) islets ($n = 6$ replicates using islet from three *Scn3a*$^{+/−}$ and five *Scn3a*$^{−/−}$ mice). *$P < 0.05$, **$P < 0.01$ vs. 1 mM glucose (same mouse strain) and $^{††}P < 0.01$ for comparison between *Scn3a*$^{+/−}$ and *Scn3a*$^{−/−}$ islets. B, as in A but comparing α-*Scn9a*$^{+/−}$ ($n = 11$ replicates using islet from three mice) and α-*Scn9a*$^{−/−}$ islets ($n = 6$ replicates using islets from five mice). *$P < 0.05$; **$P < 0.01$ vs. 1 mM glucose. C, as in A but insulin was measured. *$P < 0.05$ vs. 1 mM glucose (same strain); $^{†}P < 0.05$ vs. wild-type. D, as in C but measurements were made in β-*Scn9a*$^{+/−}$ and β-*Scn9a*$^{−/−}$ islets ($n = 5$–6 replicates using islets from five *Scn9a*$^{+/−}$ and seven *Scn9a*$^{−/−}$ mice). *$P < 0.05$ vs. 1 mM glucose (same strain).

```
NP_061340   MAMLPPPGPQSFVHFTKQSLALIEQRISEEKAKGHKDEKKDDEEEGPKPSSDLEAGKQLP 60
AAI72147    MAMLPPPGPQSFVHFTKQSLALIEQRISEEKAKGHKDEKKDDEEEGPKPSSDLEAGKQLP 60
Brain isoA  MAMLPPPGPQSFVHFTKQSLALIEQRISEEKAKGHKDEKKDDEEEGPKPSSDLEAGKQLP 60
Islet isoA  MAMLPPPGPQSFVHFTKQSLALIEQRISEEKAKGHKDEKKDDEEEGPKPSSDLEAGKQLP 60
Brain isoB  MAMLPPPGPQSFVHFTKQSLALIEQRISEEKAKGHKDEKKDDEEEGPKPSSDLEAGKQLP 60
Islet isoB  MAMLPPPGPQSFVHFTKQSLALIEQRISEEKAKGHKDEKKDDEEEGPKPSSDLEAGKQLP 60
            ************************************************************

NP_061340   FIYGDIPPGMVSEPLEDLDPYYADKKTFIVLNKGKAIFRFNATPALYMLSPFSPLRRISI 120
AAI72147    FIYGDIPPGMVSEPLEDLDPYYADKKTFIVLNKGKAIFRFNATPALYMLSPFSPLRRISI 120
Brain isoA  FIYGDIPPGMVSEPLEDLDPYYADKKTFIVLNKGKAIFRFNATPALYMLSPFSPLRRISI 120
Islet isoA  FIYGDIPPGMVSEPLEDLDPYYADKKTFIVLNKGKAIFRFNATPALYMLSPFSPLRRISI 120
Brain isoB  FIYGDIPPGMVSEPLEDLDPYYADKKTFIVLNKGKAIFRFNATPALYMLSPFSPLRRISI 120
Islet isoB  FIYGDIPPGMVSEPLEDLDPYYADKKTFIVLNKGKAIFRFNATPALYMLSPFSPLRRISI 120
            ************************************************************
                         S1
NP_061340   KILVHSLFSMLIMCTILTNCILTMTMSNPPDWTKNVEYTFTGIYTFESLIKILARGFCVGE 180
AAI72147    KILVHSLFSMLIMCTILTNCILTMTMSNPPDWTKNVEYTFTGIYTFESLIKILARGFCVGE 180
Brain isoA  KILVHSLFSMLIMCTILTNCILTMTMSNPPDWTKNVEYTFTGIYTFESLIKILARGFCVGE 180
Islet isoA  KILVHSLFSMLIMCTILTNCILTMTMSNPPDWTKNVEYTFTGIYTFESLIKILARGFCVGE 180
Brain isoB  KILVHSLFSMLIMCTILTNCILTMTMSNPPDWTKNVEYTFTGIYTFESLIKILARGFCVGE 180
Islet isoB  KILVHSLFSMLIMCTILTNCILTMTMSNPPDWTKNVEYTFTGIYTFESLIKILARGFCVGE 180
            ************************************************************
                     S2          S3              S4
NP_061340   FTFLRDPWNWLDFVVIVFAYLTEFVNLGNVSALRTFRVLRALKTISVIPGLKTIVGALIQ 240
AAI72147    FTFLRDPWNWLDFVVIVFAYLTEFVNLGNVSALRTFRVLRALKTISVIPGLKTIVGALIQ 240
Brain isoA  FTFLRDPWNWLDFVVIVFAYLTEFVNLGNVSALRTFRVLRALKTISVIPGLKTIVGALIQ 240
Islet isoA  FTFLRDPWNWLDFVVIVFAYLTEFVNLGNVSALRTFRVLRALKTISVIPGLKTIVGALIQ 240
Brain isoB  FTFLRDPWNWLDFVVIVFAYLTEFVNLGNVSALRTFRVLRALKTISVIPGLKTIVGALIQ 240
Islet isoB  FTFLRDPWNWLDFVVIVFAYLTEFVNLGNVSALRTFRVLRALKTISVIPGLKTIVGALIQ 240
            ************************************************************
                        S5
NP_061340   SVKKLSDVMILTVFCLSVFALIGLQLFMGNLKHKCFRKDLEQNETLENGHKGYQRKCKVK 300
AAI72147    SVKKLSDVMILTVFCLSVFALIGLQLFMGNLKHKCFRKDLEQNETLESIMS--TAESEEE 298
Brain isoA  SVKKLSDVMILTVFCLSVFALIGLQLFMGNLKHKCFRKDLEQNETLESIMS--TAESEEE 298
Islet isoA  SVKKLSDVMILTVFCLSVFALIGLQLFMGNLKHKCFRKDLEQNETLESIMS--TAESEEE 298
Brain isoB  SVKKLSDVMILTVFCLSVFALIGLQLFMGNLKHKCFRKDLEQNETLESIMS--TAESEEE 298
Islet isoB  SVKKLSDVMILTVFCLSVFALIGLQLFMGNLKHKCFRKDLEQNETLESIMS--TAESEEE 298
            *******************************************  .    .  .::  :

NP_061340   TMGYFYYLEGSKDALLCGFSTDSGQCPEGYECVTAGRNPDYGYTSFDTFGWAFLALFRLM 360
AAI72147    LKRYFYYLEGSKDALLCGFSTDSGQCPEGYECVTAGRNPDYGYTSFDTFGWAFLALFRLM 358
Brain isoA  LKRYFYYLEGSKDALLCGFSTDSGQCPEGYECVTAGRNPDYGYTSFDTFGWAFLALFRLM 358
Islet isoA  LKRYFYYLEGSKDALLCGFSTDSGQCPEGYECVTAGRNPDYGYTSFDTFGWAFLALFRLM 358
Brain isoB  LKRYFYYLEGSKDALLCGFSTDSGQCPEGYECVTAGRNPDYGYTSFDTFGWAFLALFRLM 358
Islet isoB  LKRYFYYLEGSKDALLCGFSTDSGQCPEGYECVTAGRNPDYGYTSFDTFGWAFLALFRLM 358
            ***  ********************************************************
                            S6
NP_061340   TQDYWENLYQQTLRAAGKTYMIFFVVVIFLGSFYLINLILAVVAMAYEEQNQANIEEAKQ 420
AAI72147    TQDYWENLYQQTLRAAGKTYMIFFVVVIFLGSFYLINLILAVVAMAYEEQNQANIEEAKQ 418
Brain isoA  TQDYWENLYQQTLRAAGKTYMIFFVVVIFLGSFYLINLILAVVAMAYEEQNQANIEEAKQ 418
Islet isoA  TQDYWENLYQQTLRAAGKTYMIFFVVVIFLGSFYLINLILAVVAMAYEEQNQANIEEAKQ 418
Brain isoB  TQDYWENLYQQTLRAAGKTYMIFFVVVIFLGSFYLINLILAVVAMAYEEQNQANIEEAKQ 418
Islet isoB  TQDYWENLYQQTLRAAGKTYMIFFVVVIFLGSFYLINLILAVVAMAYEEQNQANIEEAKQ 418
            ************************************************************

NP_061340   KELEFQQMLDRLKKEQEEAEVVFIITNTKAKQVGQRIMGLSESSSETSRLSSKAKERRN 480
AAI72147    KELEFQQMLDRLKKEQEEAEAIAAAAAEYTSLGRSRIMGLSESSSETSRLSSKAKERRN 478
Brain isoA  KELEFQQMLDRLKKEQEEAEAIAAAAAEYTSLGRSRIMGLSESSSETSRLSSKAKERRN 478
Islet isoA  KELEFQQMLDRLKKEQEEAEAIAAAAAEYTSLGRSRIMGLSESSSETSRLSSKAKERRN 478
Brain isoB  KELEFQQMLDRLKKEQEEAEAIAAAAAEYTSLGRSRIMGLSESSSETSRLSSKAKERRN 478
Islet isoB  KELEFQQMLDRLKKEQEEAEAIAAAAAEYTSLGRSRIMGLSESSSETSRLSSKAKERRN 478
            ********************* .:   :   :.  .*************************

NP_061340   RRKKKKQKLSSGEEKGDDEKLSKSGSEESIRKKSFHLGVEGHHRAREKRLSTPNQSPLSI 540
AAI72147    RRKKKKQKLSSGEEKGDDEKLSKSGSEESIRKKSFHLGVEGHHRAREKRLSTPNQSPLSI 538
Brain isoA  RRKKKKQKLSSGEEKGDDEKLSKSGSEESIRKKSFHLGVEGHHRAREKRLSTPNQSPLSI 538
Islet isoA  RRKKKKQKLSSGEEKGDDEKLSKSGSEESIRKKSFHLGVEGHHRAREKRLSTPNQSPLSI 538
Brain isoB  RRKKKKQKLSSGEEKGDDEKLSKSGSEESIRKKSFHLGVEGHHRAREKRLSTPNQSPLSI 538
Islet isoB  RRKKKKQKLSSGEEKGDDEKLSKSGSEESIRKKSFHLGVEGHHRAREKRLSTPNQSPLSI 538
            ************************************************************

NP_061340   RGSLFSARRSSRTSLFSFKGRGRDLGSETEFADDEHSIFGDNESRRGSLFVPHRPRERRS 600
AAI72147    RGSLFSARRSSRTSLFSFKGRGRDLGSETEFADDEHSIFGDNESRRGSLFVPHRPRERRS 598
Brain isoA  RGSLFSARRSSRTSLFSFKGRGRDLGSETEFADDEHSIFGDNESRRGSLFVPHRPRERRS 598
Islet isoA  RGSLFSARRSSRTSLFSFKGRGRDLGSETEFADDEHSIFGDNESRRGSLFVPHRPRERRS 598
Brain isoB  RGSLFSARRSSRTSLFSFKGRGRDLGSETEFADDEHSIFGDNESRRGSLFVPHRPRERRS 598
Islet isoB  RGSLFSARRSSRTSLFSFKGRGRDLGSETEFADDEHSIFGDNESRRGSLFVPHRPRERRS 598
            ************************************************************

NP_061340   SNISQASRSPPVLPVNGKMHSAVDCNGVVSLVDGPSALMLPNGQLLPE----------G 649
AAI72147    SNISQASRSPPVLPVNGKMHSAVDCNGVVSLVDGPSALMLPNGQLLPEVIIDKATSDDSG 658
Brain isoA  SNISQASRSPPVLPVNGKMHSAVDCNGVVSLVDGPSALMLPNGQLLPEVIIDKATSDDSG 658
Islet isoA  SNISQASRSPPVLPVNGKMHSAVDCNGVVSLVDGPSALMLPNGQLLPEVIIDKATSDDSG 658
Brain isoB  SNISQASRSPPVLPVNGKMHSAVDCNGVVSLVDGPSALMLPNGQLLPE----------G 647
Islet isoB  SNISQASRSPPVLPVNGKMHSAVDCNGVVSLVDGPSALMLPNGQLLPE----------G 647
            ***********************************************          *

NP_061340   TTNQMRKKRLSSSYFLSEDMLNDPHLRQRAMSRASILTNTVEELEESRQKCPPWWYRFAH 709
AAI72147    TTNQMRKKRLSSSYFLSEDMLNDPHLRQRAMSRASILTNTVEELEESRQKCPPWWYRFAH 718
Brain isoA  TTNQMRKKRLSSSYFLSEDMLNDPHLRQRAMSRASILTNTVEELEESRQKCPPWWYRFAH 718
Islet isoA  TTNQMRKKRLSSSYFLSEDMLNDPHLRQRAMSRASILTNTVEELEESRQKCPPWWYRFAH 718
Brain isoB  TTNQMRKKRLSSSYFLSEDMLNDPHLRQRAMSRASILTNTVEELEESRQKCPPWWYRFAH 707
Islet isoB  TTNQMRKKRLSSSYFLSEDMLNDPHLRQRAMSRASILTNTVEELEESRQKCPPWWYRFAH 707
            ************************************************************

NP_061340   TFLIWNCSPYWIKFKKFIY 728
AAI72147    TFLIWNCSPYWIKFKKFIY 737
Brain isoA  TFLIWNCSPYWIKFKKFIY 737
Islet isoA  TFLIWNCSPYWIKFKKFIY 737
Brain isoB  TFLIWNCSPYWIKFKKFIY 726
Islet isoB  TFLIWNCSPYWIKFKKFIY 726
            *******************
```

Figure 11. Predicted amino acid sequences of Na$_v$1.7 α subunits from mouse brain and islets

Amino acid sequences of splice variants of *Scn9a* from mouse brain and pancreatic islets are shown as a Clustal W alignment. Alternative mouse splice forms found in GenBank (NP_061340, 1975 amino acids; and AAI72147, 1984 amino acids) are shown as references. Identical residues are marked with asterisks. Putative transmembrane segments (S1–S6) are highlighted with continuous lines on top. Sequences of both Na$_v$1.7 α subunit isoforms from islets were identical to those expressed in brain and the GenBank sequence AAI72147, except the region highlighted. Isoform A (isoA) contains the sequence encoded by extended exon 12 (extension highlighted), while isoform B (isoB) contains the sequence encoded by conventional exon 12. Note that only the sequences of domain I and the cytoplasmic loop between domains I and II are shown because the rest of the protein is 100% identical in all isoforms.

this current is small compared to that which can be evoked from hyperpolarised membrane potentials, its magnitude is comparable to that of the voltage-gated Ca^{2+} current. Thus, it is likely to contribute to action potential firing. Indeed, we found that that action potential height is reduced by TTX. Insulin exocytosis is steeply voltage-dependent (Gopel *et al.* 2004) and it is possible that a 4–6 mV reduction of action potential height accounts for much of the suppression of glucose-induced insulin secretion produced by TTX at high (20 mM) glucose concentrations.

Electrophysiological characterization of *Scn3a* and *Scn9a* knockout mice suggests that Na$_v$1.3 represents the *functionally* important Na$^+$ channel subtype in β-cells. This conclusion is underlined by the strong reduction of glucose-induced insulin secretion in *Scn3a*$^{-/-}$ islets. Na$^+$ currents at physiological resting potentials are observed in only 30% of β-cells, but it is possible that very small Na$_v$1.3 Na$^+$ currents (too small to be detected) may be present in the remaining 70% of cells and contribute to the initiation and upstroke of the action potentials. Because of the high input resistance of the β-cell in the presence of glucose (Ashcroft & Rorsman, 2004), even such small Na$^+$ currents may have a dramatic depolarising effect on the β-cell membrane potential. At high glucose concentrations when K$_{ATP}$ channel activity is low in all β-cells, initiation of Na$_v$1.3 Na$^+$ channel-dependent electrical activity in a subset of cells may, via current spread through the gap junctions, trigger Ca^{2+}-dependent electrical activity in neighbouring β-cells in which Na$_v$1.7 Na$^+$ channels are completely inactivated. These considerations suggest that Na$_v$1.3 channels, despite their low copy number, may play a previously unrecognised modulatory role in glucose-induced electrical activity and insulin secretion in mouse β-cells.

In human β-cells, Na$^+$ channels play a prominent role in action potential generation and insulin secretion is TTX sensitive (Misler *et al.* 1992; Braun *et al.* 2008). Our data suggest that Na$_v$1.7 is indeed present in human β-cells and inactivates at hyperpolarised voltages ($\sim$−105 mV). However, consistent with the relatively low expression of *SCN9A* in β-cells (25% of all Na$^+$ channel transcripts; Nica *et al.* 2013), it comprises only a small component of the total current. The fact that non-Na$_v$1.7 currents

dominate in human β-cells can explain why their Na$^+$ currents inactivate at physiological membrane potentials.

Ablation of Na$_v$1.7 (*Scn9a*) in mice had little effect on glucose-induced insulin secretion, consistent with the fact that this current is completely inactivated at resting membrane potentials. Thus, the physiological role of Na$_v$1.7, which accounts for 80–90% of the total Na$^+$ current, in β-cells is obscure.

Role of Na$^+$ channels in α-cells

The effects of the Na$^+$ channel blocker TTX on glucagon secretion and α-cell electrical activity confirm that voltage-gated Na$^+$ channels are important for the upstroke of the α-cell action potential. Application of TTX resulted in a ~15 mV reduction of action potential height (from +2 to −12 mV). The inhibitory effect of TTX on glucagon secretion in wild-type islets is quantitatively similar to that

Figure 12. Voltage dependence of inactivation in mouse and human β-cells

A, as in Fig. 2*B* but using β-cells that only contained a Na$^+$ current component inactivating at negative membrane potentials. The inactivation curves were recorded immediately after establishment of the whole-cell configuration (●) and 15 min later (○). Data are mean ± SEM recorded in the same cells at two different times ($n = 3$). *B*, voltage dependence of Na$^+$ current inactivation in human β-cells that contained one (●, $n = 5$) or two (○, $n = 4$) components of inactivation when cells were held at −180 mV. The curves represent single (black) or double (grey) Boltzmann fits to the data (all cells from one organ donor).

produced by genetically ablating *Scn3a*$^{-/-}$. This argues that Na$_v$1.3 represents the functionally important Na$^+$ channel in α-cells. Because of the steep voltage dependence of exocytosis in α-cells, the reduction in action potential height produced by TTX can be expected to exert a large inhibitory effect (75%) on exocytosis (Zhang *et al.* 2013), sufficient to account for the suppression of glucagon secretion.

As in β-cells, Na$_v$1.7 is unlikely to contribute to action potential firing or glucagon secretion because of its inactivation properties. This idea is supported by the finding that ablation of Na$_v$1.7 has little effect on glucagon secretion.

Human α-cells possess a similar complement of Na$^+$ channel subunits, and other ion channels, to human β-cells (Ramracheya *et al.* 2010; Nica *et al.* 2013). The question therefore arises as to why glucose stimulates insulin secretion, but inhibits glucagon secretion. We have argued elsewhere that this is principally because the magnitude of the K$_{ATP}$ conductance is much smaller in α-cells (Ashcroft & Rorsman, 2013; Zhang *et al.* 2013). As a consequence, α-cells are electrically active at low glucose concentrations and membrane potential-dependent inactivation of Na$^+$ channels mediated by glucose will have a strong inhibitory effect on electrical activity and glucagon secretion. In β-cells Na$^+$ channel inactivation also occurs, but the stimulatory effect on glucose on electrical activity (and thus secretion) dominates.

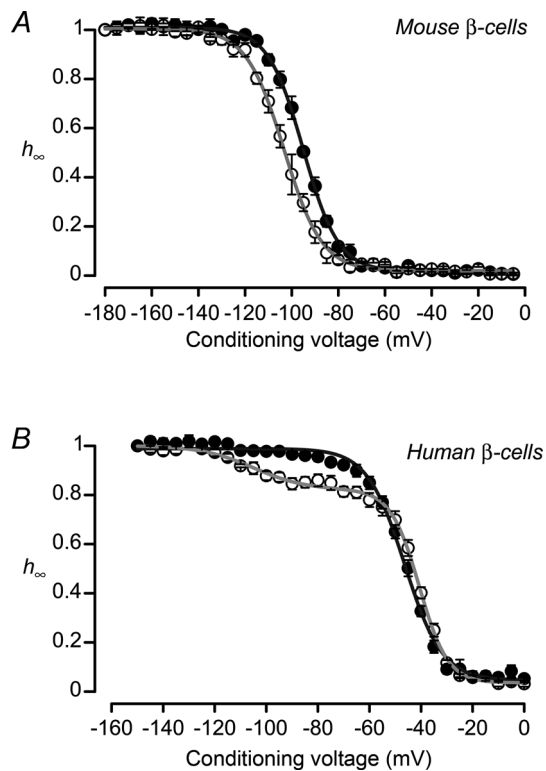### Why do β-cell Na$_v$1.7 channels inactivate at unphysiologically hyperpolarised potentials?

In β-cells, inactivation of Na$_v$1.7 proceeds at such negative voltages that very few (if any) of these channels remain 'activatable' at the normal resting potential (−70 mV). Why this is the case is an enigma. Mouse Na$_v$1.7 currents in dorsal root ganglion cells inactivate with a $V_{0.5}$ of ~−70 mV (Herzog *et al.* 2003), ~30 mV more positive than the corresponding value in β-cells. This puzzling difference does not reflect expression of a splice variant because the β-cell Na$_v$1.7 sequence is identical to that found in neurones. This argues that there must be something in β-cells that shifts inactivation towards negative membrane potentials. The identity of this factor remains unknown. However, the fact that Na$_v$1.7 inactivation does not shift towards more depolarised potentials following extended intracellular dialysis suggests the involvement of a non-diffusible factor.

We speculate that the atypical inactivation of Na$_v$1.7 in islet cells results from the interaction of Na$_v$1.7 with a protein (or lipid) present in β-cells but not in neurones. We can exclude a role of Na$^+$ channel β subunits

because inactivation of the $Na_v1.3$-independent current component (representing $Na_v1.7$) was identical ($V_{0.5}$ at -100 mV) in α- and β-cells despite these two cell types expressing β_3 and β_1 subunits, respectively. It is notable that $Na_v1.3$ and $Na_v1.6$ (as suggested by the Na^+ current measurements in human β-cells; Fig. 12) channels undergo voltage-dependent inactivation at physiological membrane potentials. Thus, the impact of this modulation appears specific for $Na_v1.7$ channels. The nature of this modulator remains to be determined. $Na_v1.7$ channels play a key role in pain sensation (Dib-Hajj *et al.* 2008), and thus identification of the putative modulator might provide a new target for therapeutic drugs directed at alleviating pain.

References

Ashcroft F & Rorsman P (2004). Type 2 diabetes mellitus: not quite exciting enough? *Hum Mol Genet* **13**(Spec No 1), R21–31.

Ashcroft FM & Rorsman P (2012). Diabetes mellitus and the β cell: the last ten years. *Cell* **148**, 1160–1171.

Ashcroft FM & Rorsman P (2013). K-ATP channels and islet hormone secretion: new insights and controversies. *Nat Rev Endocrinol* **9**, 660–669.

Bengtsson M, Stahlberg A, Rorsman P & Kubista M (2005). Gene expression profiling in single cells from the pancreatic islets of Langerhans reveals lognormal distribution of mRNA levels. *Genome Res* **15**, 1388–1392.

Braun M, Ramracheya R, Amisten S, Bengtsson M, Moritoh Y, Zhang Q, Johnson PR & Rorsman P (2009). Somatostatin release, electrical activity, membrane currents and exocytosis in human pancreatic delta cells. *Diabetologia* **52**, 1566–1578.

Braun M, Ramracheya R, Bengtsson M, Clark A, Walker JN, Johnson PR & Rorsman P (2010). Gamma-aminobutyric acid (GABA) is an autocrine excitatory transmitter in human pancreatic beta-cells. *Diabetes* **59**, 1694–1701.

Braun M, Ramracheya R, Bengtsson M, Zhang Q, Karanauskaite J, Partridge C, Johnson PR & Rorsman P (2008). Voltage-gated ion channels in human pancreatic β-cells: electrophysiological characterization and role in insulin secretion. *Diabetes* **57**, 1618–1628.

Catterall WA (2000). From ionic currents to molecular mechanisms: the structure and function of voltage-gated sodium channels. *Neuron* **26**, 13–25.

Catterall WA, Goldin AL & Waxman SG (2005). International Union of Pharmacology. XLVII. Nomenclature and structure–function relationships of voltage-gated sodium channels. *Pharmacol Rev* **57**, 397–409.

Chera S, Baronnier D, Cigliola V, Jensen JN, Gu G, Ghila L, Furuyama K, Thorel F, Gribble F, Reimann F & Herrera PL (2014). Diabetes recovery by age-dependent conversion of pancreatic δ-cells into insulin producers. *Nature* doi:10.1038/nature13633.

Cox JJ, Reimann F, Nicholas AK, Thornton G, Roberts E, Springell K, Karbani G, Jafri H, Mannan J, Raashid Y, Al-Gazali L, Hamamy H, Valente EM, Gorman S, Williams R, McHale DP, Wood JN, Gribble FM & Woods CG (2006). An SCN9A channelopathy causes congenital inability to experience pain. *Nature* **444**, 894–898.

De Marinis YZ, Salehi A, Ward CE, Zhang Q, Abdulkader F, Bengtsson M, Braha O, Braun M, Ramracheya R, Amisten S, Habib AM, Moritoh Y, Zhang E, Reimann F, Rosengren AH, Shibasaki T, Gribble F, Renstrom E, Seino S, Eliasson L & Rorsman P (2010). GLP-1 inhibits and adrenaline stimulates glucagon release by differential modulation of N- and L-type Ca^{2+} channel-dependent exocytosis. *Cell Metab* **11**, 543–553.

Dib-Hajj SD, Yang Y & Waxman SG (2008). Genetics and molecular pathophysiology of $Na_v1.7$-related pain syndromes. *Adv Genet* **63**, 85–110.

Dunning BE, Foley JE & Ahren B (2005). Alpha cell function in health and disease: influence of glucagon-like peptide-1. *Diabetologia* **48**, 1700–1713.

Ernst SJ, Aguilar-Bryan L & Noebels JL (2009). Sodium channel $\beta1$ regulatory subunit deficiency reduces pancreatic islet glucose-stimulated insulin and glucagon secretion. *Endocrinology* **150**, 1132–1139.

Goldin AL, Barchi RL, Caldwell JH, Hofmann F, Howe JR, Hunter JC, Kallen RG, Mandel G, Meisler MH, Netter YB, Noda M, Tamkun MM, Waxman SG, Wood JN & Catterall WA (2000). Nomenclature of voltage-gated sodium channels. *Neuron* **28**, 365–368.

Girard CA, Wunderlich FT, Shimomura K, Collins S, Kaizik S, Proks P, Abdulkader F, Clark A, Ball V, Zubcevic L, Bentley L, Clark R, Church C, Hugill A, Galvanovskis J, Cox R, Rorsman P, Bruning JC & Ashcroft FM. (2009). Expression of an activating mutation in the gene encoding the KATP channel subunit Kir6.2 in mouse pancreatic beta cells recapitulates neonatal diabetes. *J Clin Invest* **119**, 80–90 doi:10.1172/JCI35772.

Gonoi T & Hille B (1987). Gating of Na channels – inactivation modifiers discriminate among models. *J Gen Physiol* **89**, 253–274.

Gopel S, Kanno T, Barg S, Galvanovskis J & Rorsman P (1999). Voltage-gated and resting membrane currents recorded from β-cells in intact mouse pancreatic islets. *J Physiol* **521**, 717–728.

Gopel S, Zhang Q, Eliasson L, Ma XS, Galvanovskis J, Kanno T, Salehi A & Rorsman P (2004). Capacitance measurements of exocytosis in mouse pancreatic α-, β- and δ-cells within intact islets of Langerhans. *J Physiol* **556**, 711–726.

Gopel SO, Kanno T, Barg S & Rorsman P (2000*a*). Patch-clamp characterisation of somatostatin-secreting δ-cells in intact mouse pancreatic islets. *J Physiol* **528**, 497–507.

Gopel SO, Kanno T, Barg S, Weng XG, Gromada J & Rorsman P (2000*b*). Regulation of glucagon release in mouse α-cells by K_{ATP} channels and inactivation of TTX-sensitive Na^+ channels. *J Physiol* **528**, 509–520.

Hauge-Evans AC, King AJ, Carmignac D, Richardson CC, Robinson IC, Low MJ, Christie MR, Persaud SJ & Jones PM (2009). Somatostatin secreted by islet δ-cells fulfills multiple roles as a paracrine regulator of islet function. *Diabetes* **58**, 403–411.

Henquin JC & Meissner HP (1984). Significance of ionic fluxes and changes in membrane potential for stimulus-secretion coupling in pancreatic B-cells. *Experientia* **40**, 1043–1052.

Herrera PL (2000). Adult insulin- and glucagon-producing cells differentiate from two independent cell lineages. *Development* **127**, 2317–2322.

Herzog RI, Cummins TR, Ghassemi F, Dib-Hajj SD & Waxman SG (2003). Distinct repriming and closed-state inactivation kinetics of Na$_v$1.6 and Na$_v$1.7 sodium channels in mouse spinal sensory neurons. *J Physiol* **551**, 741–750.

Hille B (2001). *Ion Channels of Excitable Membranes*. Sinauer Associates, Sunderland, MA.

Kanno T, Rorsman P & Gopel SO (2002). Glucose-dependent regulation of rhythmic action potential firing in pancreatic β-cells by K$_{ATP}$-channel modulation. *J Physiol* **545**, 501–507.

Koopmann TT, Bezzina CR & Wilde AA (2006). Voltage-gated sodium channels: action players with many faces. *Ann Med* **38**, 472–482.

Lou XL, Yu X, Chen XK, Duan KL, He LM, Qu AL, Xu T & Zhou Z (2003). Na$^+$ channel inactivation: a comparative study between pancreatic islet β-cells and adrenal chromaffin cells in rat. *J Physiol* **548**, 191–202.

Macdonald PE, Marinis YZ, Ramracheya R, Salehi A, Ma X, Johnson PR, Cox R, Eliasson L & Rorsman P (2007). A K$_{ATP}$ channel-dependent pathway within α cells regulates glucagon release from both rodent and human islets of Langerhans. *PLoS Biol* **5**, e143.

Misler S, Barnett DW, Gillis KD & Pressel DM (1992). Electrophysiology of stimulus-secretion coupling in human β-cells. *Diabetes* **41**, 1221–1228.

Nassar MA, Baker MD, Levato A, Ingram R, Mallucci G, McMahon SB & Wood JN (2006). Nerve injury induces robust allodynia and ectopic discharges in Na$_v$1.3 null mutant mice. *Mol Pain* **2**, 33.

Nica AC, Ongen H, Irminger JC, Bosco D, Berney T, Antonarakis SE, Halban PA & Dermitzakis ET (2013). Cell-type, allelic, and genetic signatures in the human pancreatic beta cell transcriptome. *Genome Res* **23**, 1554–1562.

Nassar MA, Stirling LC, Forlani G, Baker MD, Matthews EA, Dickenson AH & Wood JN. (2004). Nociceptor-specific gene deletion reveals a major role for Nav1.7 (PN1) in acute and inflammatory pain. *Proc Natl Acad Sci U S A* **101**, 12706–12711 doi:10.1073/pnas.0404915101.

Plant TD (1988). Na$^+$ currents in cultured mouse pancreatic B-cells. *Pflugers Arch* **411**, 429–435.

Postic C, Shiota M, Niswender KD, Jetton TL, Chen Y, Moates JM, Shelton KD, Lindner J, Cherrington AD & Magnuson MA (1999). Dual roles for glucokinase in glucose homeostasis as determined by liver and pancreatic β cell-specific gene knock-outs using Cre recombinase. *J Biol Chem* **274**, 305–315.

Pressel DM & Misler S (1990). Sodium channels contribute to action potential generation in canine and human pancreatic islet B cells. *J Membr Biol* **116**, 273–280.

Raj A, Peskin CS, Tranchina D, Vargas DY & Tyagi S (2006). Stochastic mRNA synthesis in mammalian cells. *PLoS Biol* **4**, e309.

Ramracheya R, Ward C, Shigeto M, Walker JN, Amisten S, Zhang Q, Johnson PR, Rorsman P & Braun M (2010). Membrane potential-dependent inactivation of voltage-gated ion channels in α-cells inhibits glucagon secretion from human islets. *Diabetes* **59**, 2198–2208.

Renstrom E, Ding WG, Bokvist K & Rorsman P (1996). Neurotransmitter-induced inhibition of exocytosis in insulin-secreting β cells by activation of calcineurin. *Neuron* **17**, 513–522.

Rocheleau JV, Remedi MS, Granada B, Head WS, Koster JC, Nichols CG & Piston DW (2006). Critical role of gap junction coupled KATP channel activity for regulated insulin secretion. *PLoS Biol* **4**, e26.

Rorsman P, Eliasson L, Kanno T, Zhang Q & Gopel S (2011). Electrophysiology of pancreatic beta-cells in intact mouse islets of Langerhans. *Progr Biophys Mol Biol* **107**, 224–235.

Stahlberg A & Bengtsson M (2010). Single-cell gene expression profiling using reverse transcription quantitative real-time PCR. *Methods* **50**, 282–288.

Strowski MZ, Kohler M, Chen HY, Trumbauer ME, Li Z, Szalkowski D, Gopal-Truter S, Fisher JK, Schaeffer JM, Blake AD, Zhang BB & Wilkinson HA (2003). Somatostatin receptor subtype 5 regulates insulin secretion and glucose homeostasis. *Mol Endocrinol* **17**, 93–106.

Vignali S, Leiss V, Karl R, Hofmann F & Welling A (2006). Characterization of voltage-dependent sodium and calcium channels in mouse pancreatic A- and B-cells. *J Physiol* **572**, 691–706.

Zhang Q, Bengtsson M, Partridge C, Salehi A, Braun M, Cox R, Eliasson L, Johnson PR, Renstrom E, Schneider T, Berggren PO, Gopel S, Ashcroft FM & Rorsman P. (2007). R-type Ca(2+)-channel-evoked CICR regulates glucose-induced somatostatin secretion. *Nat Cell Biol* **9**, 453–460 doi:10.1038/ncb1563.

Zhang Q, Galvanovskis J, Abdulkader F, Partridge CJ, Gopel SO, Eliasson L & Rorsman P (2008). Cell coupling in mouse pancreatic β-cells measured in intact islets of Langerhans. *Phil Trans R Soc A* **366**, 3503–3523.

Zhang Q, Ramracheya R, Lahmann C, Tarasov A, Bengtsson M, Braha O, Braun M, Brereton M, Collins S, Galvanovskis J, Gonzalez A, Groschner LN, Rorsman NJ, Salehi A, Travers ME, Walker JN, Gloyn AL, Gribble F, Johnson PR, Reimann F, Ashcroft FM & Rorsman P (2013). Role of K$_{ATP}$ channels in glucose-regulated glucagon secretion and impaired counterregulation in type 2 diabetes. *Cell Metab* **18**, 871–882.

Additional information

Competing interests

The authors declare that they have no conflict of interest.

Author contributions

Funding

Acknowledgements